JNeurosci
THE JOURNAL OF NEUROSCIENCE



***Research Articles: Cellular/Molecular***

# Antagonizing increased miR-135a levels at the chronic stage of experimental TLE reduces spontaneous recurrent seizures

**Vamshidhar R. Vangoor[1], Cristina R. Reschke[2,3], Ketharini Senthilkumar[1], Lieke L. van de Haar[1], Marina de Wit[1], Giuliano Giuliani[1], Mark H. Broekhoven[1], Gareth Morris[2,3,4], Tobias Engel[2], Gary P. Brennan[2,3], Ronan M. Conroy[5], Peter C. van Rijen[6], Peter H. Gosselaar[6], Stephanie Schorge[4], Roel Q. J. Schaapveld[7], David C. Henshall[2,3], Pierre N. E. De Graan[1] and R. Jeroen Pasterkamp[1]**

[1]*Department of Translational Neuroscience, UMC Utrecht Brain Center, University Medical Center Utrecht, Utrecht University, 3584 CG Utrecht, The Netherlands.*

[2]*Department of Physiology and Medical Physics, Royal College of Surgeons in Ireland, Dublin, D02, Ireland.*

[3]*FutureNeuro Research Centre, Royal College of Surgeons in Ireland, Dublin, D02, Ireland.*

[4]*Department of Clinical and Experimental Epilepsy, Institute of Neurology, University College London, WC1N 3BG, London, UK.*

[5]*Department of Epidemiology and Public Health Medicine, Royal College of Surgeons in Ireland, Dublin D02 YN77, Ireland.*

[6]*Department of Neurosurgery, UMC Utrecht Brain Center, University Medical Center Utrecht, 3584 CG, Utrecht, The Netherlands*

[7]*InteRNA Technologies B.V., Yalelaan 62, 3584 CM Utrecht, The Netherlands.*

https://doi.org/10.1523/JNEUROSCI.3014-18.2019

Received: 29 November 2018

Revised: 31 March 2019

Accepted: 16 April 2019

Published: 23 April 2019

**Author contributions:** V.V., C.R., K.S., L.L.v.d.H., G.G., G.M., D.C.H., P.d.G., and J.P. designed research; V.V., C.R., K.S., L.L.v.d.H., M.d.W., G.G., M.H.B., G.M., T.E., and G.P.B. performed research; V.V., C.R., K.S., L.L.v.d.H., M.d.W., G.G., M.H.B., G.M., G.P.B., R.C., and J.P. analyzed data; V.V. and J.P. wrote the paper; P.v.R., P.H.G., S.S., and R.S. contributed unpublished reagents/analytic tools.

**Conflict of Interest:** The authors declare no competing financial interests.

This work was supported by funding from the European Union's 7th Framework Programme under grant agreement No [602130], EpimiRNA and Dutch Epilepsiefonds (WAR 12-08, 15-05), and Netherlands Organization for Scientific Research (ALW-VICI) (to RJP). We would like to thank Prof. Jorgen Kjems for providing the pJEBB vector backbone and Prof. Gerhard Schratt for the Mef2-vp16 vector.

**Correspondence should be addressed to** corresponding author: Department of Translational Neuroscience, UMC Utrecht Brain Center, University Medical Center Utrecht, Utrecht University, 3584 CG Utrecht, The Netherlands. Email: r.j.pasterkamp@umcutrecht.nl

**Cite as:** J. Neurosci 2019; 10.1523/JNEUROSCI.3014-18.2019

# Antagonizing increased miR-135a levels at the chronic stage of experimental TLE reduces spontaneous recurrent seizures

Vamshidhar R. Vangoor[1], Cristina R. Reschke[2, 3, 8], Ketharini Senthilkumar[1, 8], Lieke L. van de Haar[1], Marina de Wit[1], Giuliano Giuliani[1], Mark H. Broekhoven[1], Gareth Morris[2, 3, 4], Tobias Engel[2], Gary P. Brennan[2, 3], Ronan M. Conroy[5], Peter C. van Rijen[6], Peter H. Gosselaar[6], Stephanie Schorge[4], Roel Q. J. Schaapveld[7], David C. Henshall[2, 3], Pierre N. E. De Graan[1], R. Jeroen Pasterkamp[1*]

[1] Department of Translational Neuroscience, UMC Utrecht Brain Center, University Medical Center Utrecht, Utrecht University, 3584 CG Utrecht, The Netherlands. [2] Department of Physiology and Medical Physics, Royal College of Surgeons in Ireland, Dublin, D02, Ireland. [3] FutureNeuro Research Centre, Royal College of Surgeons in Ireland, Dublin, D02, Ireland. [4] Department of Clinical and Experimental Epilepsy, Institute of Neurology, University College London, WC1N 3BG, London, UK. [5] Department of Epidemiology and Public Health Medicine, Royal College of Surgeons in Ireland, Dublin D02 YN77, Ireland. [6] Department of Neurosurgery, UMC Utrecht Brain Center, University Medical Center Utrecht, 3584 CG, Utrecht, The Netherlands [7] InteRNA Technologies B.V., Yalelaan 62, 3584 CM Utrecht, The Netherlands. [8] These authors contributed equally.

* corresponding author: Department of Translational Neuroscience, UMC Utrecht Brain Center, University Medical Center Utrecht, Utrecht University, 3584 CG Utrecht, The Netherlands. Email: r.j.pasterkamp@umcutrecht.nl

Abbreviated title: Mechanism and therapeutic effect of miR-135a in TLE

Number of pages: 49 Figures: 7 Tables: 4
Number of words in abstract: 234 Introduction: 646 Discussion: 1500

**Acknowledgements**
This work was supported by funding from the European Union's 7th Framework Programme under grant agreement No [602130], EpimiRNA and Dutch Epilepsiefonds (WAR 12-08, 15-05), and Netherlands Organization for Scientific Research (ALW-VICI) (to RJP). We would like to thank Prof. Jorgen Kjems for providing the pJEBB vector backbone and Prof. Gerhard Schratt for the Mef2-vp16 vector.

**Conflict of Interest**
R.Q.J.S. is a shareholder in InteRNA Technologies B.V. R.Q.J.S. is stock option holders in InteRNA Technologies B.V. The remaining authors declare no competing financial interests.

**Author contributions**
V.R.V., C.R.R., K.S., L.L.v.d.H., G.G., G.M., D.C.H., P.N.E.d.G., and R.J.P. designed research; V.R.V., C.R.R., K.S., L.L.v.d.H., M.d.W., G.G., M.H.B., G.M., T.E., and G.P.B performed research; P.C.v.R., P.H.G., provided human resected mTLE tissue; S.S., and R.Q.J.S. contributed unpublished reagents/analytic tools; V.R.V., C.R.R., K.S., L.L.v.d.H., M.d.W., G.G., G.M., G.P.B., R.M.C. and R.J.P. analyzed data; V.R.V and R.J.P. wrote the paper.

**Abstract**

Mesial Temporal Lobe Epilepsy (mTLE) is a chronic neurological disease characterized by recurrent seizures. The anti-epileptic drugs currently available to treat mTLE are ineffective in one-third of patients and lack disease-modifying effects. MicroRNAs (miRNAs), a class of small non-coding RNAs which control gene expression at the post-transcriptional level, play a key role in the pathogenesis of mTLE and other epilepsies. Although manipulation of miRNAs at acute stages has been reported to reduce subsequent spontaneous seizures, it is uncertain whether targeting miRNAs at chronic stages of mTLE can also reduce seizures. Furthermore, the functional role and downstream targets of most epilepsy-associated miRNAs remain poorly understood. Here, we show that miR-135a is selectively upregulated within neurons in epileptic brain and report that targeting miR-135a *in vivo* using antagomirs after onset of spontaneous recurrent seizures can reduce seizure activity at the chronic stage of experimental mTLE in male mice. Further, by using an unbiased approach combining immunoprecipitation and RNA sequencing, we identify several novel neuronal targets of miR-135a, including Mef2a. Mef2 proteins are key regulators of excitatory synapse density. Mef2a and miR-135a show reciprocal expression regulation in human (of both sexes) and experimental TLE, and miR-135a regulates dendritic spine number and type through Mef2. Together, our data show that miR-135a is target for reducing seizure activity in chronic epilepsy, and that deregulation of miR-135a in epilepsy may alter Mef2a expression and thereby affect synaptic function and plasticity.

Keywords: Epilepsy, Mesial Temporal Lobe Epilepsy, miRNA, Antagomirs, RNA sequencing

75 **Significance statement**

76

77 miRNAs are post-transcriptional regulators of gene expression with roles in the pathogenesis
78 of epilepsy. However, the precise mechanism-of-action and therapeutic potential of most
79 epilepsy-associated miRNAs remain poorly understood. Our study reveals dramatic
80 upregulation of the key neuronal miRNA miR-135a in both experimental and human mTLE.
81 Silencing miR-135a in experimental TLE reduces seizure activity at the spontaneous
82 recurrent seizure stage. These data support the exciting possibility that miRNAs can be
83 targeted to combat seizures after spontaneous seizure activity has been established. Further,
84 by using unbiased approaches novel neuronal targets of miR-135a, including members of the
85 Mef2 protein family, are identified that begin to explain how deregulation of miR-135a may
86 contribute to epilepsy.

87 **Introduction**

88

89 Epilepsy is a chronic neurological disease that is characterized by recurrent unprovoked
90 seizures and that affects 65 million people worldwide (Chang and Lowenstein, 2003; Moshé
91 et al., 2015). Temporal Lobe Epilepsy (TLE) is a subclass of epilepsy and accounts for about
92 one third of all epilepsies (Engel, 2001). It consists of several subgroups of which Mesial
93 Temporal Lobe Epilepsy with Hippocampal Sclerosis (mTLE-HS) is most severe and is
94 resistant to pharmacological treatment (Wieser, 2004). For many mTLE-HS patients, surgical
95 removal of the hippocampus is the only effective treatment for achieving seizure control
96 (Semah et al., 1998; Blümcke et al., 2013). While anti-convulsant and anti-epileptic drugs are
97 used to treat mTLE patients, these drugs reduce the occurrence of seizures but do not treat the
98 underlying pathophysiology. Hence there is an urgent need to develop novel treatment
99 strategies for treating TLE and other epilepsies (Löscher et al., 2013).

100 The pathological mechanisms underlying mTLE are still incompletely understood, but
101 animal models of epilepsy and human tissue studies suggest that epileptogenesis involves a
102 cascade of molecular and cellular network alterations (Becker et al., 2003; Staley, 2004;
103 Wetherington et al., 2008; Rakhade and Jensen, 2009). During the past several years,
104 microRNAs (miRNAs) have emerged as important post-transcriptional regulators of gene
105 expression, providing a completely new level of control over gene expression. miRNAs are
106 small, non-coding RNAs (18-25 nucleotides long) that are generated from longer RNA
107 precursors transcribed from the genome. miRNAs recognize complementary target sequences
108 in cognate mRNAs and inhibit protein expression by either destabilizing their mRNA targets
109 or by inhibiting protein translation (Kosik, 2006; Bartel, 2018). A single miRNA can have
110 many different targets and it can regulate several genes in a pathway or single genes in
111 multiple pathways (Ebert and Sharp, 2012; Bartel, 2018). Thus, miRNAs may be employed

112 to robustly disrupt single pathways or to simultaneously interfere with multiple pathways
113 (Ebert and Sharp, 2012; Henshall et al., 2016).

114 Deregulation of miRNAs has been linked to several of the pathological mechanisms
115 underlying TLE (Aronica et al., 2010; Kan et al., 2012; Jimenez-Mateos and Henshall, 2013;
116 Gorter et al., 2014; Cattani et al., 2016). Manipulation of fourteen of the sixteen miRNAs that
117 have been functionally validated *in vivo* has been found to elicit beneficial effects at the
118 histopathology level and on seizure activity (Gross et al., 2016; Henshall et al., 2016; Iori et
119 al., 2017). Despite this progress, the mechanisms through which most miRNAs affect
120 seizures and/or epileptogenesis remain unknown. Furthermore, whether manipulation of
121 miRNAs at later, chronic stages of epilepsy has therapeutic effects is an important but largely
122 unresolved question. Previously, we have shown that a significant number of miRNAs are
123 up- or down-regulated in hippocampal tissue of human mTLE patients (Kan et al., 2012). Of
124 those miRNAs, miR-135a is of particular interest as it is known to control neuronal
125 morphology and synaptic function. For example, miR-135a modulates glutamatergic
126 neurotransmission by regulating Complexin1/2 in the amygdala (Mannironi et al., 2017).
127 Furthermore, miR-135a promotes developmental axon growth and branching, cortical
128 neuronal migration, and regeneration of retinal ganglion cell (RGC) axons following optic
129 nerve injury in adult mice (van Battum et al., 2018). Because of these biological effects of
130 miR-135a and the strong increase in miR-135a in mTLE patients, we further investigated the
131 potential role of miR-135a in mTLE pathogenesis. Our data show that miR-135a expression
132 is specifically increased during the chronic stage of experimental TLE and that inhibiting
133 miR-135a at this stage reduces spontaneous seizure activity. These data show one of the first
134 examples that inhibiting a miRNA at chronic stages of experimental TLE has therapeutic
135 effects on spontaneous seizure activity. As a first step towards understanding how miR-135a
136 influences seizure activity we identify the activity-dependent transcription Mef2a as a direct

137 neuronal miR-135a target. Further, our results confirm reciprocal regulation of miR-135a and
138 Mef2a expression in epilepsy and reveal that miR-135a can regulate dendritic spine
139 morphology and number through Mef2.

140 **Materials and Methods**

141

142 **Animals**

143 All animal experiments were performed according to the institutional guidelines and
144 approved by 1) the Research Ethics Committee of the Royal College of Surgeons in Ireland
145 (RCSI). RCSI Ethics: REC 842; and HPRA (Health Products Regulatory Authority)
146 AE19127/P001, or 2) the local ethical animal experimentation committee (Dierexperimenten
147 Ethische Commissie) of the University Medical Center Utrecht (protocol numbers DEC
148 2014.I.01.005, 527-16-532-03-07). C57bl6J mice (male and female) were obtained from
149 Charles Rivers Laboratories.

150

151 **Intra-amygdala kainate mouse model**

152 Animals were handled according to institutional guidelines and experiments were reviewed
153 and approved by RCSI (REC 842), under a license from the Department of Health (HPRA,
154 AE19127/001), Dublin, Ireland and reviewed and approved by the ethical animal
155 experimentation committee (Dierexperimenten Ethische Commissie) of University Medical
156 Center Utrecht under the project license AVD115002016532 (protocol number 527-16-532-
157 03-07). Status epilepticus (SE) induction, EEG recording and analysis were performed as
158 previously described (Mouri et al., 2008; Jimenez-Mateos et al., 2012). Briefly, for the long-
159 term monitoring (24/7 video/EEG), male mice were implanted with telemetric EEG
160 transmitters (Data Systems International (DSI)) for bilateral recording on both brain
161 hemispheres with four measuring electrodes. EEG data was acquired using Ponemah
162 acquisition software (version 5.20, DSI) system and F20-EET EEG transmitters (DSI) were
163 used. For PBS/scrambled control experiments, EEG data was acquired only unilaterally using
164 the Dataquest A.R.T$^{TM}$ Gold acquisition software (Version 4.33, DSI) system and TA11ETA-

165 F10 EEG transmitters (DSI). Two measuring electrodes were affixed over the dorsal
166 hippocampi/temporal cortex (coordinates 2.0 mm posterior to Bregma and 1.5 mm from the
167 midline) and over the cerebellum midline. In both experiments, two days after mice
168 underwent surgery SE was induced by the intra-amygdala administration of kainic acid (0.3
169 μg in 0.2 μl in PBS). Control animals received the same volume of PBS. Forty minutes after
170 microinjection, mice received an intraperitoneal injection of lorazepam (8 mg/kg) to reduce
171 morbidity and mortality. Mice were video/EEG monitored for 24 h to confirm they were
172 presented with similar SE.
173
174 **Intracerebroventricular injections**
175 For antagomirs, intracerebroventricular (i.c.v) injections were performed as described
176 (Jimenez-Mateos et al., 2012; Reschke et al., 2017). From day 7 after SE induction, an
177 epileptic baseline EEG was recorded. At day 14 (D14) mice received an infusion of 1.0
178 nmol/2 μl of antagomir-135a (ant-135a) LNA modified and 3'-cholesterol-modified
179 oligonucleotides (Exiqon) in PBS. Controls received the same volume of PBS. Similarly, for
180 control experiments 1.0 nmol/1 μl of scrambled (Scr) LNA modified and 3'-cholesterol-
181 modified oligonucleotides (Exiqon) in PBS was injected, and compared with controls that
182 received the same volume of PBS. During this period mice were continuously EEG and video
183 monitored for another week. EEG data analysis was performed using Neuroscore (Verison
184 2.1.0 DSI) and LabChart 8 software (ADInstruments Ltd).
185
186 **RNA isolation and quantitative PCR**
187 Hippocampal tissue samples from pharmaco-resistant mTLE patients were obtained as
188 described previously (Kan et al., 2012), at the University Medical Center Utrecht. Informed
189 consent was obtained from all patients for procedures approved by the Institutional ethics

190 board. Post-mortem human tissue material was obtained from the Netherlands Brain Bank.
191 Samples from seven patients (male and female) with mTLE-HS (with hippocampal sclerosis)
192 and eight post-mortem control samples (male and female) were used (Table 1). Patient tissue
193 representing all hippocampal regions was selected using Nissl staining. Approximately 20 mg
194 of tissue was collected by slicing 25 μm thick sections on a cryostat. For intra-amygdala
195 kainate (IAK) mice, hippocampus was dissected, frozen and stored at -80$^{o}$C. Total RNA was
196 isolated using the miRNeasy kit (Qiagen), according to the manufacturer's instructions. RNA
197 quantity was determined using Nanodrop (Thermo Scientific). For miRNA quantitative PCR
198 (qPCR), first strand cDNA synthesis was performed using a universal cDNA synthesis kit
199 (Exiqon) according to the manufacturer's recommendation. QPCR reactions were run in a
200 Quantstudio 6 flex Real-Time PCR system (Applied Biosystems) using microRNA LNA$^{TM}$
201 PCR primer sets (miR-135a, miR-124) and SYBR Green master mix (Exiqon). For pre-
202 miRNA qPCR, primer sequences (pre-miR-135a1 and a2) were designed using Primer3
203 software. Primer sequences for each target are provided in Table 2. 100 ng of RNA was
204 reverse transcribed using Superscript III first strand synthesis kit (Thermo fischer scientific).
205 Similarly, for validation of bio-IP targets 100 ng of inputs RNA and equal amount of IP RNA
206 was reverse transcribed as above. QPCR reactions were run on Quantstudio 6 flex Real-Time
207 PCR system (Applied Biosystems) using Fast start universal SYBR Green master mix
208 (Roche). All samples were run in duplicates. Ct values were determined using Quant studio
209 real time pcr software v1.1. For miRNA, expression levels were estimated by normalizing to
210 5s rRNA. Pre-miRs were normalized to GAPDH (human) and β-actin (mouse). For Bio-ip
211 fold enrichment of target gene in the IP sample was estimated after normalizing to input
212 deltaCt. DeltaCt and fold changes were calculated and the statistical significance was
213 analyzed by Mann Whitney U test and Students *t* test. $P < 0.05$ was considered as significant.
214

215 **Non-radioactive *in situ* hybridisation**

216 Non-radioactive *in situ* hybridization was performed as described previously (Kan et al.,
217 2012). Three patients from each group (control and mTLE) were used for *in situ*
218 hybridization. Similarly, for IAK mice sections three mice per group were used. Briefly, 16
219 µm thick sections from fresh frozen hippocampal tissue were collected on glass slides and
220 stored at -80$^{o}$C until use. Sections were fixed (4% PFA for 10 min at RT), acetylated (10 min
221 at RT) and treated with proteinase K (5 µg/ml for 5 min at RT). Pre-hybridisation was
222 performed for 1 h at RT. Hybridisation was performed with 10 nM of double-DIG (3' and
223 5')-labeled locked nucleic acid (LNA) probe for human-miR-135a-5p (Exiqon) or LNA-DIG
224 scrambled-miR probe overnight at 50$^{o}$C. Slides were washed at 55$^{o}$C in 0.2x SSC for 1 h,
225 followed by blocking with 10% fetal calf serum (FCS) in B1 buffer (0.1 M Tris pH 7.5, 0.15
226 M NaCl) for 1 h at RT. For ISH on antagomir injected mice, a custom-made double DIG
227 labeled miR-135a inhibitor (miR-135a.inh) probe (Exiqon) that specifically recognizes ant-
228 135a was used. Hybridisation was performed with 20 nM of miR-135a.inh probe overnight at
229 55$^{o}$C followed by stringency washes at 60$^{o}$C in B1 buffer. Sections were incubated with anti-
230 digoxigenin-AP Fab fragments (1;2500, Roche Diagnostics) in 10% FCS in B1 buffer
231 overnight at 4$^{o}$C. Slides were treated with 5-bromo-4-chloro-3-indolyl phosphate (BCIP) and
232 nitrobluetetrazolium (NBT) substrates (NBT/BCIP stock solution, Roche Diagnostics) in B3
233 (0.1 M Tris pH 9.5, 0.1 M NaCl, 50 mM $MgCl_2$) for 5–20 h at RT. Staining was stopped by
234 washes in PBS and slides were mounted using vectashield (VectorLabs). No staining was
235 observed in sections hybridized with scramble probe. Images were acquired with brightfield
236 microscope and processed using ImageJ.

237 A similar protocol was used for FISH except that hybridization was performed at 55$^{o}$C and
238 washes at 60$^{o}$C. After blocking, slides were co-incubated with anti-Digoxigenin-POD (1;500,
239 Roche Diagnostics) and mouse anti-NeuN (1;400, Millipore, RRID:AB_2298772) or rabbit

240 anti-GFAP (1;1000, Dako Cytomation, RRID:AB_10013482) antibodies overnight at 4°C.
241 Signal was amplified using the TSA™ Cyanine 3 System (1;50 in amplification diluent,
242 PerkinElmer) for 10 min at RT. After washes with PBS, slides were incubated with
243 secondary antibodies (Alexafluor 488, Alexafluor 647; Invitrogen) against the primary
244 antibody for 1.5 h at RT. Nuclei were stained with DAPI (4′,6-diamidino-2-phenylindole) for
245 10 min at RT and slides were mounted using ProLong Gold (Life Technologies). Images
246 were acquired using a confocal laser scanning microscope (LSM880, Zeiss) and processed
247 using ImageJ.
248
249 **RNA co-immunoprecipitation with biotinylated mimics**
250 N2A cells were cultured in Dulbecco's modified Eagle's medium (DMEM) low glucose
251 supplemented with L-glutamine, penicillin/streptomycin (100 U/ml and 100 mg/ml,
252 respectively) and 10% FCS (Invitrogen) at 37°C with 5% $CO_2$. For each condition (miR-
253 135a, negative control (NC-1) and no transfection) three 10 cm dishes with 2x10^6 cells/dish
254 were plated and transfected with 37.5 nM of 3' biotinylated miRNA mimics (miR-135a and
255 NC-1: Dharmacon) using HighPerfect Transfection reagent (Qiagen). RNA co-
256 immunoprecipitation was performed as described previously (Wani and Cloonan, 2014) with
257 some modifications. Briefly, 24 h after transfection cells were collected and lysed in lysis
258 buffer (10 mM Tris-Cl pH 7.5, 10 mM KCl, 1.5 mM Mgcl2, 5mM DTT, 0.5% NP-40, 60
259 U/ml SUPERase-in RNase inhibitor (Invitrogen), protease inhibitor tablet (Roche) in MQ)
260 and the cleared cell lysates were incubated with Dynabeads M-280 Streptavidin beads
261 (Invitrogen) for 30 min at RT. Beads were washed three times in wash buffer (lysis buffer
262 containing 1 M NaCl) and stored in Qiazol at -80°C. Total RNA was extracted using
263 miRNeasy kit (Qiagen). One part of the beads was incubated with 4x Nu-PAGE sample
264 buffer (with 10% β-mercaptoethanol in MQ) for 10 min at 70°C to extract bound proteins.

265 Proteins were then separated in a 8% SDS-PAGE gel and the subsequent transferred blot was
266 incubated with rabbit anti-Ago2 antibody (1;1000, Cell Signaling, RRID:AB_2096291) and
267 mouse anti-β-actin (1;2000, Sigma-Aldrich, RRID:AB_476743) in blocking solution (5%
268 Milk in 1x TBS-T) overnight at 4$^{o}$C, finally signal was detected as above.
269

270 **Library preparation and total RNA sequencing**

271 For input samples, libraries for total RNA sequencing were prepared using the TruSeq
272 Stranded Total RNA (w/RiboZero Gold) sample prep kit (Illumina). The starting material
273 (100 ng) of total RNA was depleted of rRNAs using Ribo-Zero Gold (removes both
274 cytoplasmic and mitochondrial rRNA) magnetic bead-based capture-probe system (Illumina).
275 The remaining RNA, including mRNAs, lincRNAs and other RNA species, was subsequently
276 purified (RNAcleanXP) and enzymatically fragmentated. For IP samples, libraries were
277 prepared using the TruSeq stranded mRNA sample prep kit (Illumina) according to the
278 manufacturer's instructions with some modifications: the starting material (37.5 – 50.0 ng) of
279 total RNA was not mRNA-enriched nor fragmented prior to library synthesis. First strand
280 synthesis and second strand synthesis were performed and double stranded cDNA was
281 purified (Agencourt AMPure XP, Beckman Coulter). The cDNA was end repaired, 3'
282 adenylated and Illumina sequencing adaptors were ligated onto the fragments ends, and the
283 library was purified (Agencourt AMPure XP). The polyA+ RNA stranded libraries were pre-
284 amplified with PCR and purified (Agencourt AMPure XP). Library size distribution was
285 validated and quality inspected using the 2100 Bioanalyzer (high sensitivity DNA chip,
286 Agilent). High quality libraries were quantified using the Qubit Fluorometer (Life
287 Technologies). Single-end sequencing was performed using the NextSeq500 instrument
288 according to the manufacturer's instructions (Illumina).
289

290 **Read mapping and differential expression analysis**

291 Following trimming of low-quality bases and adapter sequences with FASTQ-MCF (version
292 0.0.13), processed reads were mapped to the GRCm38.p6 reference mouse genome
293 (Ensembl) with TopHat2 (version 2.0.13). 'fr-secondstrand' option was chosen for the
294 alignments of the total RNA sequencing data. Mapped counts were summarised for each gene
295 using the python script htseq-count (Anders et al., 2015). For differential expression analysis,
296 count data for genes and transcripts were analysed for differential expression in R using the
297 Bioconductor package EdgeR version 3.12.1 (Robinson et al., 2010) with the trimmed mean
298 of M-values (TMM) normalisation method (Robinson and Oshlack, 2010). Gene expression
299 levels were corrected for batch effects by including the series of sequencing rounds. Adjusted
300 *P* values for multiple testing were calculated using the Benjamini-Hochberg false discovery
301 rate (FDR) and only genes with an FDR < 0.05 were considered significantly differentially
302 expressed. Data visualisation was performed in R using the ggplot2 library (version 2.1.0).
303 Gene expression heatmaps with hierarchical clustering of expression profiles were created in
304 R with the Bioconductor pheatmap package. Enrichment analysis was performed using the R
305 package goseq (Young et al., 2010) to correct for bias due to transcript length. All the raw
306 and processed RNAseq data is deposited at NCBI Gene Expression Omnibus (GEO) with
307 reference number GSE123000.
308 https://www.ncbi.nlm.nih.gov/geo/query/acc.cgi?acc=GSE123000 (reviewer password:
309 ubarweoaptgbreb).

310

311 ***In silico* prediction of miRNAs binding sites**

312 miRanda software version 3.3a was used to predict microRNA signatures. The following
313 parameters were used in this study: match with a minimum threshold score of 150; target

314 mRNA duplex with minimum folding free energy threshold -7kcal/mol; gap opening penalty
315 -8; gap extension penalty -2; scaling parameter 4 for complementary nucleotide match score.
316

317 **Target Validation: Luciferase assay and Western blotting**

318 HEK293 (RRID:CVCL_0045) and N2A (RRID:CVCL_0470) cells were cultured according
319 to the guidelines provided by ATCC. Luciferase assays were performed in HEK293 cells and
320 target validations by western blot were performed in N2A cells.

321 For luciferase assays, miRNA recognition elements (MRE) for miR-135a present in
322 the 3' UTR of Mef2a were identified in RNAseq data and also predicted by Targetscan.
323 Oligonucleotides with these sites were cloned into the psi-Check2 vector (Promega).
324 Oligonucleotides with WT (MEF2A-135a-fw: TCG AGA GCA GAA CCT TGG AAA AAA
325 AAA GCC ATG GC, Rv-GGC CGC CAT GGC TTT TTT TTT CCA AGG TTC TGC TC)
326 and MUT (MEF2A-135aM-fw: TCG AGA GCA GAA CCT TGG AAA AAA AAA GGC
327 TTG GC; Rv- GGC CGC CAA GCC TTT TTT TTT CCA AGG TTC TGC TC) miR-135a
328 binding sites were phosphorylated, annealed and ligated into the *NotI* and *XhoI* sites of the
329 multiple cloning site. Cells (8x10^4) were transfected using Lipofectamine 2000 (Invitrogen)
330 with 250 ng of reporter construct together with 25 pmol of miRIDIAN miRNA mimic or
331 Negative control (NC-1, Dharmacon), a non-targeting negative control mimic from *C.*
332 *elegans*. Cells were harvested after 24 h and luciferase assays were performed using the dual-
333 luciferase assay system (E1960, Promega) on a Luminometer. Normalization against Renilla
334 luciferase activity was used to determine relative luciferase activity.

335 For protein analysis, western blotting was performed. N2A cells were transfected with
336 miRIDIAN mimics for miR-135a or a negative control using Lipofectamine 2000. After 48 h
337 cells were harvested and lysed in RIPA buffer (50 mM Tris pH.7.5, 150 mM Nacl, 0.5% NP-
338 40, 0.5% NaDoc, 1% Triton, Protease inhibitor (Roche) in MilliQ (MQ)). Equal amounts of

339 protein samples were separated in SDS-PAGE gels (8%) and transferred onto nitrocellulose
340 blotting membranes (GE Healthcare Lifesciences), following which blots were blocked for 1
341 h at RT in 5 % milk powder in 1xTBS-Tween. Blots were incubated overnight at 4$^{o}$C with
342 rabbit-anti-NR3C1 (GR) (1;1000, Santa-cruz Biotechnology, RRID:AB_2155786), rabbit-
343 anti-PlxnA4 (1;250, Abcam, RRID:AB_944890), mouse-anti-β actin (1;2000, Sigma-
344 Aldrich, RRID:AB_476743). Blots were stained with peroxidase-conjugated secondary
345 antibodies for 1 h at RT and signal was detected by incubating blots with Pierce ECL
346 substrate (Thermo Fischer Scientific). Images were acquired using a FluorChem M imaging
347 system (Protein Simple). Using ImageJ, individual band intensities for each sample were
348 measured and normalized to corresponding β-actin levels. Statistical significance of the
349 relative expression between conditions of each protein was estimated by t test (GraphPad
350 Prism version 6 software, RRID:SCR_002798). Except for Mef2a experiments, blots were
351 blocked in Supermix blocking solution (Tris 50 mM, NaCl 154 mM, 0.25% gelatin, 0.5%
352 Triton-x-100 in MQ, pH 7.4) for 10 min at RT and incubated overnight at 4$^{o}$C with rabbit
353 anti-Mef2a (1;50,000, Abcam, RRID:AB_10862656) and mouse anti-β actin (1;2000, Sigma-
354 Aldrich, RRID:AB_476743). Blots were washed in 1x TBS-Tween and incubated with
355 secondary antibodies coupled with IR dyes (anti-rabbit-IRdye 800 1;5000 and anti-mouse-
356 IRdye700 1;2000 in 1x TBS-Tween) for 1 h at RT. Finally, blots were washed in 1x TBS-
357 Tween and scanned on Odyssey Clx imaging system (LI-COR biosciences, Westburg) using
358 Li-COR Image studio v3.1 software (RRID:SCR_015795) and band intensities were
359 measured and statistical significance of the relative expression between conditions was
360 estimated by t test (GraphPad Prism version 6 software, RRID:SCR_002798).
361
362 **Immunohistochemistry and Western blotting for Mef2a**

363 Mef2a immunostainings were performed on resected human hippocampal mTLE sections and
364 2 wk IAK mouse tissue and compared to corresponding controls. 16 µm sections were
365 blocked in 3% NGS, 0.2% Triton in 1x PBS (pH 7.4) for 1 h at RT followed by incubation in
366 anti-Mef2a antibody (1;150, Abcam) and anti-NeuN antibody (1;400, Millipore) in blocking
367 solution overnight at 4$^{o}$C. Sections were washed and incubated with corresponding Alexa-
368 fluor conjugated (Thermofischer scientific) secondary antibodies for 1.5 h at RT, followed by
369 washes in 1x PBS and stained for nuclei with DAPI and mounted using ProLong gold
370 (Thermofischer scientific). High resolution images were acquired using a confocal
371 microscope (LSM880, Zeiss) and processed using ImageJ. For measuring Mef2a
372 fluorescence intensities in ant-135a and control mice, confocal images from the CA3 region
373 were acquired using similar settings for both groups. Internal densities (IntDen) were
374 estimated by using the particle analysis plugin on ImageJ.

375 For analyzing Mef2a protein levels in human mTLE and IAK mice hippocampal
376 tissue, protein lysates were prepared in RIPA buffer and equal amounts of proteins were
377 separated in SDS-PAGE gels (8% gel for mouse samples and 10% gel for human samples),
378 and transferred onto nitrocellulose membranes, blocked and incubated overnight at 4$^{o}$C with
379 rabbit anti-Mef2a (for human 1;20000, for mice 1;50000, Abcam, RRID:AB_10862656) and
380 mouse anti-β-actin (1;2000, Sigma-Aldrich, RRID:AB_476743). Blots were stained,
381 developed and quantified as described above.

382

383 **Culturing and transfection of primary mouse hippocampal neurons**

384 Dissociated hippocampal neurons were cultured as described previously (Van Battum et al.,
385 2014). Briefly, C57bl6J (P0-1) mouse (male or female) pups were decapitated and brains
386 were quickly isolated in ice cold dissection medium (Leibovitz's L-15 supplemented with 7
387 mM HEPES (Thermo scientific)). Hippocampus was isolated, trypsinized in 0.25% trypsin in

388 L15-HEPES medium for 20 min at 37°C, followed by trituration using fire polished Pasteur
389 pipettes in growth medium (Neurobasal medium supplemented with B27,
390 Penicillin/streptomycin, L-glutamine and β-mercaptoethanol). Dissociated cells were plated
391 onto glass coverslips coated with PDL (20 $\mu gml^{-1}$) and laminin (40 $\mu gml^{-1}$) in growth
392 medium and incubated at 37°C with 5% $CO_2$. Half of the growth medium was refreshed twice
393 a week. On day *in vitro* (DIV)14 neurons were transfected with 0.5 µg of pre-miR-135a1
394 (cloned into the pJEBB vector with CMV promoter, contains GFP reporter) or pJEBB vector
395 only. For rescue experiments, pJEBB-pre-miR-135a1 and the constitutively active mutant
396 Mef2-vp16 (Fiore et al., 2009) were co-transfected. Transfected neurons were fixed on
397 DIV16 with 4% PFA and 4% sucrose in PBS for 20 min. Immunocytochemistry was
398 performed by blocking neurons in blocking buffer (4% NGS, 0.1% BSA, 0.1% Triton-X-100
399 in 1x PBS (pH-7.4)) for 1 h at RT followed by incubation with primary antibody chicken
400 anti-GFP (1;1000, Abcam, RRID:AB_300798) diluted in blocking buffer. The next day
401 washes in 1x PBS were performed followed by incubation with appropriate secondary
402 antibodies in blocking buffer for 1 h at RT. Sections were mounted using ProLong Gold
403 (Thermo Fischer Scientific). High resolution images were acquired using an oil immersion
404 63x objective of a confocal laser scanning microscope (LSM880, Zeiss). 6-7 Z stack images
405 of each apical dendrites close to the soma were captured. Using ImageJ software
406 (RRID:SCR_003070) with cell counter plugin, different types of spines categorized as
407 immature to mature: filopodium, thin, stubby, mushroom and cupshaped on secondary
408 dendrite were identified and counted. Spine density was determined by dividing the number
409 of spines on a branch with the length of the branch.
410

411 **Experimental design and statistical analysis**

412 C57bl6J mice were used in this study. Statistical analysis was performed using GraphPad
413 Prism (version 7.05, RRID: SCR_002798) and a *P* value <0.05 was considered as significant
414 for all statistical tests. Seizure frequencies before (baseline) and after ant-135a were analyzed
415 using paired t test, the number of seizures per day using F statistics mixed design repeated
416 measures general linear model. Seizure duration and total time spent in seizures were
417 analyzed using t test. Differences between two groups were tested using either two tailed t
418 test or Wilcoxon Mann Whitney test. For comparing more than two groups one-way ANOVA
419 was used. Exact *P* values, t-values and degrees of freedom are provided in the text and the n
420 in the figure legend.
421 In our previous study, miR-135a was found to be upregulated in mTLE-HS condition using
422 microarray (Kan et al., 2012). We started with validating the expression of miR-135a in a
423 different set of hippocampal human patient samples and tested for both mature and pre-miR-
424 135a levels (Fig. 1A, 2E). n = 8 controls and 7 patient RNA samples were used and analyzed
425 statistically using unpaired two tailed t test. Further, LNA ISH and FISH were performed to
426 establish cell type-specificity. At least three patient tissue samples were used for ISH (Fig.
427 1B).
428 Next, we checked if the expression of miR-135a is also regulated in experimental TLE in an
429 intra-amygdala kainate (IAK) model. Only male mice were used for inducing SE, as
430 previously described (Mouri et al., 2008; Jimenez-Mateos et al., 2012). Hippocampi from
431 four PBS and three KA mice were used to test the expression levels of mature miR-135a and
432 pre-miR-135a by qPCR at 2 wk after SE (Fig. 2A, 2F), unpaired t test was performed for
433 statistics. Changes in expression were also confirmed by ISH at 24 h and 2 wk after SE (Fig.
434 2B), and cell type-specificity was determined by FISH (Fig. 2C) in at least three IAK and
435 control mice. DAPI positive cell number in the DG supra and infrapyramidal blades was
436 estimated using the ImageJ cell counter plugin in a similar region of interest (ROI) in KA and

437 PBS control mice. Statistical analysis was performed using Student's t-test and n=3 mice per
438 group were used.

439 Next, to understand if *in vivo* targeting of miR-135a in epileptic mice can alter seizure
440 occurrence, SE induced mice were treated with antagomirs. First, we confirmed whether ant-
441 135a is able to reduce endogenous levels of miR-135a at a given dose without any off-target
442 effects (Fig. 3A), and tested localization of ant-135a in the hippocampus using a LNA ISH
443 probe designed to recognize ant-135a (Fig. 3B). One-way ANOVA was used for statistics to
444 compare differences between groups, n = 3 mice per group were used for qPCR and ISH.

445 For *in vivo* ant-135a experiments, ten mice were implanted with guide cannulas, EEG
446 transmitters and SE was induced as described previously (Jimenez-Mateos et al., 2012).
447 Similar SE induction was confirmed by performing continuous EEG recordings until 24 h
448 after SE was induced. Baseline EEG and video recordings were acquired from day 7. On day
449 14 five mice received an intra-cerebro-ventricularly (i.c.v) injection of ant-135a and five
450 controls with equal amount of PBS. Mice were then followed for one week with 24/7 EEG
451 and video recordings (Fig. 3C). Statistical difference in seizure frequency for baseline
452 recordings comparing ant-135a and control group was estimated using Wilcoxon Mann-
453 whitney statistic, and for overall difference in seizure count (Fig. 3E), F statistics with mixed
454 design repeated measures general linear model test was performed. For average seizure
455 duration and for time spent in ictal activity paired t test was performed (Fig. 3F and 3G). In
456 an independent set of animals, the effect of PBS and Scr injections on seizure activity was
457 assessed. As described above, mice implanted with guide cannulas were injected with KA.
458 On day 14, n=4 mice per group were injected with either Scr in PBS or an equal volume of
459 PBS and recorded for one week. F statistics with mixed design repeated measures general
460 linear model test was performed to analyze the results.

461 To find new binding partners for miR-135a, immunoprecipitation using biotin-tagged
462 miRNA mimics was performed. Immunoprecipitated RNA was collected from three
463 independent experiments and sent for sequencing, n = 3 samples from each group were
464 sequenced for total RNA (Fig. 4). Gene expression levels were corrected for batch effects by
465 including a series of sequencing rounds. Adjusted *P* values for multiple testing were
466 calculated using the Benjamini-Hochberg false discovery rate (FDR) and only genes with an
467 FDR < 0.05 were considered significantly differentially expressed and based on these various
468 plots were generated. Further the selected genes were validated for fold enrichment by qPCR
469 (Fig. 6A) and endogenous proteins levels of few selected targets was assessed in N2a cells.
470 Four independent transfections were performed and was repeated twice, normalized means of
471 band intensities were checked statistically using t test.
472 From the immunoprecipitations and RNA-seq data, Mef2a was selected based on its function
473 as a transcription factor regulating several downstream targets that in turn can regulate
474 activity dependent synaptic density. Direct interaction of miR-135a with Mef2a 3' UTR was
475 estimated in HEK293 cells by performing luciferase assay in two independent experiments
476 with four transfections each time (Fig 7A, B). To assess the role of miR-135a in regulating
477 neuronal spine density, we examined changes in the number of different type of spines (Fig.
478 7D) after miR-135a overexpression, and after co-transfecting a Mef2 vector that lacks the 3'
479 UTR combined with miR-135a. Mouse hippocampal neurons were used and three
480 independent transfections were performed with triplicate of wells each time for each
481 condition. A total of 54 neurons among three conditions were analyzed for different types of
482 spines. One-way ANOVA with Sidak *post hoc* test was performed (Fig. 7D, E). Next, we
483 checked if Mef2a protein levels were altered *in vivo* in mice model and in human mTLE
484 patient tissue where miR-135a expression was increased. At least four mice per group (Fig.
485 7G, H), and four patients per group (Fig. 7J, K) were used. Statistical difference was

486 estimated by Mann-Whitney U (MWU) test. Next, Mef2a immunostainings were performed
487 in IAK mice model (Fig. 7I) and in human mTLE hippocampus (Fig. 7L) using at least three
488 tissue samples per group. Finally, to check whether ant-135a treated KA mice show rescue in
489 Mef2a protein, immunostainings for Mef2a were performed (Fig. 7M) in three mice per
490 group. Fluorescence intensity of Mef2a was analyzed in the CA3 region of the hippocampus
491 (region of interest (ROI) marked in Fig. 7M), due to variable cell loss in other regions of the
492 hippocampus between conditions (Control and Ant-135a mice). Mef2a fluorescence intensity
493 was expressed as ratio of IntDen in a given area. Statistical analysis was performed by Mann-
494 Whitney U (MWU) test.

495 **Results**

496

497 **Increased expression of miR-135a in human and experimental TLE**

498 Our previous work identified miR-135a as one of the top 20 miRNAs showing increased
499 expression in hippocampal tissue resected from mTLE patients (Kan et al., 2012). Further, we
500 recently showed that miR-135a controls neuronal morphology and migration *in vitro* and *in*
501 *vivo* (van Battum et al., 2018). To begin to characterize a potential role for miR-135a in the
502 pathophysiology of TLE, miR-135a expression was assessed in human TLE hippocampus
503 (mTLE-HS) and controls. Quantitative PCR (qPCR) and *in situ* hybridization showed that
504 miR-135a expression levels were increased in mTLE hippocampus as compared to control
505 ($t_{(13)} = 3.493$, $p = 0.0040$, unpaired t test; Figure 1A), as previously shown by microarray
506 analysis (Kan et al., 2012). To verify the spatial distribution of miR-135a in human
507 hippocampal tissue, we performed *in situ* hybridization (ISH). In line with the qPCR data,
508 stronger signals for miR-135a were observed in mTLE hippocampus as compared to control.
509 Signals were mainly confined to neurons in the CA and DG regions (Figure 1B). To confirm
510 this cell type-specific localization, fluorescent ISH (FISH) was performed in combination
511 with immunohistochemistry for NeuN (neurons) or GFAP (astrocytes). MiR-135a co-
512 localized with NeuN but not GFAP, indicating that miR-135a expression is predominantly
513 neuronal (Figure 1C).

514 Next, we checked whether seizure induction (status epilepticus, SE) in an experimental
515 model of TLE (by intra-amygdala microinjection of the glutamate receptor agonist kainic
516 acid (KA)(Mouri et al., 2008)) would also lead to increased levels of miR-135a. Indeed, we
517 observed a strong increase in miR-135a expression at day 14 (D14) after SE by qPCR ($t_{(5)} =$
518 $2.811$, $p = 0.0375$, unpaired t test; Figure 2A) and ISH (Figure 2B). ISH revealed a strong
519 signal for miR-135a in the soma of pyramidal neurons in the hippocampus, and also in

520 neurons in the cortex, thalamus and amygdala at D14 (Figure 2B). In control mouse, and
521 human, hippocampus, most DG granule cells and CA pyramidal neurons displayed low-to-
522 moderate miR-135a expression. In TLE patients and 2 weeks following KA injections
523 moderate-to-high expression was found in the majority of DG and CA neurons (Fig. 1B, 2B).
524 Quantification of the number of cells in the DG region of the hippocampus did not reveal
525 significant differences in KA verssus PBS control mice (Suprapyramidal blade: PBS- 84,44 ±
526 3,52, KA- 80,33 ± 1,893. $t_{(16)}$=1.029, p=0.319, unpaired t test; Infrapyramidal blade: PBS-
527 72,44 ± 2,352, KA- 67,67 ± 3,997, $t_{(16)}$=1.03, p=0.318, unpaired t test; n=3 mice and 9
528 sections/group). This shows that the increase in miR-135a expression is not due to an
529 increase in the number of DG cells, e.g. as a result of increased adult neurogenesis. Similar to
530 our observations in human mTLE hippocampus, miR-135a was predominantly neuronal, i.e.
531 localized in neurons and not in astrocytes (Figure 2C). The mature form of miR-135a, miR-
532 135a-5p, is spliced from two different pre-transcripts in both human and mice that arise from
533 different chromosomal loci (Figure 2D). To examine whether a specific locus was
534 responsible for the increase in miR-135a expression in TLE, pre-miR levels were studied in
535 human and mouse. Pre-miR-135A2 was significantly increased in human mTLE ($t_{(11)}$ =
536 2.359, p = 0.0379, unpaired t test; Figure 2E), whereas in mice both pre-miR-135a1 and pre-
537 miR-135a2 were significantly increased (Pre-miR-135a1: $t_{(12)}$ = 4.613, p = 0.0006; Pre-miR-
538 135a2: $t_{(12)}$ = 1.828, p = 0.0462, unpaired t test; Figure 2F). In all, we found increased
539 expression of miR-135a in hippocampal neurons in TLE.
540

541 **Silencing of miR-135a reduces spontaneous recurrent seizures**

542 Our data show that, at least in a model of experimental TLE, miR-135a levels are high at the
543 time recurrent spontaneous seizures are detected. To link increased miR-135a expression to
544 spontaneous seizures, this miRNA was targeted by antagomirs (locked nucleic acid (LNA) 3′

545 cholesterol-conjugated oligonucleotides (Exiqon)). Several studies have shown that
546 antagomirs can effectively reduce the severity of SE when administered before SE induction
547 (Jimenez-Mateos et al., 2012; Gross et al., 2016; Reschke et al., 2017), or the number of
548 spontaneous seizures when administered immediately after SE (Jimenez-Mateos et al., 2012;
549 Reschke et al., 2017). However, whether administering of antagomirs in the spontaneous
550 recurrent seizure (SRS) phase can influence seizure occurrence remains poorly understood.
551 Antagomirs were administered intracerebroventricularly at different concentrations to test for
552 their specific effect on miR-135a. Twenty-four hours after injection, miR-135a levels were
553 significantly reduced at 1.0 nmol of antagomir, whereas expression of another, unrelated
554 miRNA, miR-124, was not affected. Injection of 1.5 nmol of antagomir had a small but non-
555 significant effect on miR-124 expression (vehicle vs ant-135a 1.0 nmol, $t_{(8)} = 3.545$, vehicle
556 vs ant-135a 1.5 nmol, $t_{(8)} = 3.645$, $p = 0.0214$, one-way ANOVA with Sidak *post hoc* test;
557 Figure 3A). On basis of these data injections of 1.0 nmol were used in subsequent
558 experiments. However, first ISH was used to detect ant-135a following antagomir or control
559 injection. This analysis showed that ant-135a is taken up by hippocampal neurons in the CA
560 and DG regions (Figure 3B).

561 To assess the effect of blocking miR-135 on the occurrence of spontaneous seizures,
562 SE-induced mice were injected with antagomirs for miR-135a or control at D14 and
563 continuously monitored by EEG for 7 days after injection (Figure 3C). One-week prior
564 injections (D7-D14 after SE) baseline EEG recordings were performed and no significant
565 difference in seizure frequency was observed between treated and control animals ($t_{(9)} = 0.34$,
566 $p = 0.743$, Wilcoxon Mann-Whitney test; Figure 3D-3E). We verified in an independent
567 experiment that injecting PBS or a modified scrambled (Scr) version of the antagomir in PBS
568 on D14 yielded similar seizure patterns over one week of recording (average number of
569 seizures from D14-D21: PBS = 27 and Scr = 33, mixed design repeated measures general

570 linear model; day*treatment interaction; F statistic - 0.513 ($F_{(7,21)}$ = 2.49 for $\alpha$ = 0.05);
571 *p*=0.819; n=4 mice per group). Following injection of ant-135a at D14, a significant decrease
572 in the number of SRS per day was detected (Figure 3D). A significantly different and strong
573 reduction in seizure count was observed in ant-135a treated as compared to control mice
574 (mixed design repeated measures general linear model; F statistic - 13.858 ($F_{(13,39)}$ = 1.98 for
575 $\alpha$ = 0.05); *p*<0.001; Figure 3E). The average seizure duration was not different between the
576 groups, before ant-135a injection ($t_{(4)}$ = 0.7931, p = 0.4721, paired t test), whereas it was
577 significantly lower after injection ($t_{(4)}$ = 10.22, p = 0.0005, paired t test; Figure 3F) and
578 reduced spontaneous seizures were found when analyzing EEG traces (Figure 3H). Similarly,
579 the total amount of time spent in seizures was reduced following ant-135a injection ($t_{(4)}$ =
580 7.715, p = 0.0015, paired t test; Figure 3G). Control injection at D14 caused an increase in
581 time spent in seizures, which may be due to an additional insult caused by the injection of
582 PBS. Conversely, time spent in seizures was strongly reduced following ant-135a injection
583 mice at D14 (Figure 3G). On average, ant-135a injected mice spent less time (<300 sec) in
584 seizures per day, as compared to control mice (>300 sec) (Figure 3I). Together, these data
585 show that blocking elevated expression of miR-135a during the period of recurrent
586 spontaneous seizures has an acute seizure suppressive effect.
587
588 **Identification of miR-135a targets**
589 Our previous work shows that miR-135a can affect axon growth and regeneration by
590 controlling KLF4 expression (van Battum et al., 2018). However, the acute nature of the
591 effects of ant-135a injection on seizure activity *in vivo* hints at interference with cellular
592 processes that regulate neuronal activity such as intracellular signaling, synaptic transmission
593 or synaptic morphology. miRNAs function by binding specific sequences known as miRNA
594 recognition elements (MRE) in the 3' untranslated regions (UTR) of target transcripts. Upon

595 binding, miRNAs repress translation or induce target RNA degradation. Prediction tools are
596 available that predict targets based on a few empirical rules derived experimentally
597 (Brennecke et al., 2005; Lewis et al., 2005), but many of these computational prediction tools
598 perform poorly in experimental validation due to high false positive rates (Krek et al., 2005).
599 To identify targets that are physically interacting with miR-135a, we performed miRNA
600 immunoprecipitation in neuronal mouse Neuro2A cells using biotin-tagged mimics. miR-
601 135a and scrambled mimics were tagged with a biotin molecule at their 3' end (Figure 4A,
602 B), as 3' molecule tagging was reported to not interfere with seed recognition, miRNA
603 binding and function (Ørom and Lund, 2007; Ørom et al., 2008). Although applying
604 previously reported protocols for bio-miR IP (Wani and Cloonan, 2014), we validated the IP
605 procedure by immunoblotting for Ago2 (the main component of RISC complex) following IP
606 of miR-135 and scrambled mimics. Ago2 was detected in both input and IP samples, whereas
607 the cytoskeletal protein β-actin was detected only in input samples (Figure 4C). The presence
608 of Ago2 confirms that the bio-miRNA mimic has been immunoprecipitated with the RISC
609 complex, and presumably bound RNA targets. The sequence of the negative control is based
610 on a *C. elegans* miRNA with minimal sequence identity with human, mouse and rat. The
611 presence of Ago2 in the negative control IP sample can most likely be explained by the fact
612 that Argonaute proteins are very conserved among species (Höck and Meister, 2008).

613 Following IP, total RNA sequencing was performed. For input samples, on average
614 58.5 million and for IP samples 48.7 million high quality reads were obtained. For input
615 samples, 80-90% of the reads could be aligned with the mouse reference genome, but for IP
616 samples 39.7% of reads could be aligned with the reference genome and the rest with
617 ribosomal RNA. The presence of ribosomal RNA can be explained by the lack of polyA+
618 enrichment or ribosomal RNA depletion in the sample preparation. Analysis of input samples
619 revealed only few significantly changed transcripts including validated miR-135a targets

620 such as Complexins (Cplx1 and Cplx2) (Data deposited at GEO (GSE123000)) (Hu et al.,
621 2014; Mannironi et al., 2017). In IP samples, levels of 587 transcripts were significantly
622 altered (using a cutoff of FDR<0.05 and $p$<0.01) (Figure 4D; Data deposited at GEO
623 (GSE123000)). These observations were supported by principal component analyses (PCA)
624 which showed clear segregation of gene expression profiles for IP samples (NC vs miR-135a
625 IP), but no clear segregation for inputs (Figure 4E, F). Furthermore, IP samples contained
626 many previously reported miR-135a targets (Table 3).

627 Gene ontology (GO) analysis REVIGO (Supek et al., 2011) demonstrated that
628 differentially expressed transcripts found in IP samples are involved in neuron-related
629 functions as semaphorin-plexin signaling, semaphorin receptor activity, ion transport, and
630 cAMP response element binding (Figure 5A-C). As a first step to identify targets of miR-
631 135a relevant for the observed effect of ant-miR-135a treatment *in vivo*, we selected
632 transcripts from the IP samples with predicted miR-135a MREs, using miRanda software.
633 MREs were found to be present not only in the 3'UTR (258), but also in the 5' UTR (33) and
634 the coding sequence (CDS) (279) of the 578 transcripts, 177 putative targets had no predicted
635 target site (Figure 5D; (Data deposited at GEO (GSE123000)). miR-135a and miR-135b are
636 highly similar and have an identical seed region, so in principle these miRNAs could target a
637 similar set of mRNAs (van Battum et al., 2018). Comparison of targets in IP samples of miR-
638 135a and miR-135b (not shown) revealed 50% overlap while 25.8% of targets were unique
639 for miR-135a) and 23.8% for miR-135b (Figure 5E).

640 Using the approach outlined above, we identified several new targets of miR-135a
641 with reported roles in the regulation of neuronal development and function (Table 4). For
642 further validation, 7 targets were selected on basis of their function in neurons and/or
643 implication in epilepsy (e.g., Tuberous sclerosis complex (TSC)1). All targets tested were
644 enriched in IP as compared to input samples (Figure 6A). The effect of overexpression of

645 miR-135a mimics in N2A cells on the expression of a few of the selected targets was tested
646 and showed a significant downregulation of NR3C1 (GR), PlxnA4 and Mef2a protein
647 expression (NR3C1 (GR): NC vs miR-135a, $t_{(6)} = 2.889$, $p = 0.0277$, unpaired t test; PlxnA4:
648 NC vs miR-135a, $t_{(6)} = 2.488$, $p = 0.0473$, unpaired t test; Mef2a: NC vs miR-135a, $t_{(6)} =$
649 $3.611$, $p = 0.0112$, unpaired t test; Figure 6B-D). This experiment confirms that targets
650 identified by IP can be regulated by miR-135a.
651
652 **The miR-135a target Mef2a is regulated in TLE**
653 MEF2 proteins (MEF2A-D) form a family of transcription factors that are spatially and
654 temporally expressed in the brain (Lyons et al., 1995), with most prominent expression for
655 MEF2A, 2C and 2D. MEF2s mediate activity-dependent synaptic development, and are
656 activated by neurotrophin stimulation and calcium influx resulting from increased
657 neurotransmitter release at synapses (Flavell et al., 2008). Mutations in *MEF2C* are described
658 in patients with severe mental retardation and epilepsy (Nowakowska et al., 2010; Bienvenu
659 et al., 2013). In addition, MEF2A is deregulated in the temporal cortex of epilepsy patients
660 and following experimental TLE (Huang et al., 2016). Based on our ant-135a experiments
661 (Figure 3), the reported functions of Mef2a and its deregulation in TLE, and its specific
662 enrichment by miR-135a IP, we focused subsequent experiments on Mef2a. Mef2a 3'UTR
663 contains one specific conserved binding site for miR-135a (seed sequence from 1024-1030nt)
664 (Figure 7A). This site is targeted by miR-135a as shown by luciferase assay. Co-expression
665 of miR-135a mimics with the miR-135a binding site in a luciferase reporter vector led to
666 reduced luciferase activity. Mutation of the site abolished the effect of miR-135a (Mef2a+NC
667 vs Mef2a+miR-135a: $t_{(6)} = 5.291$, $p = 0.0018$, unpaired t test; Mef2a+miR-135a vs
668 Mef2amut+miR-135a: $t_{(6)} = 3.951$, $p = 0.0075$, unpaired t test; Figure 7B).

669 Both MEF2 proteins and miR-135a have previously reported effects on synapse
670 development and function. Mef2 proteins mediate activity-dependent synaptic development
671 by regulating genes that control synapse number (Flavell et al., 2006), while miR-135 was
672 shown to promote NMDA-induced spine retraction and long-lasting spine shrinkage (Hu et
673 al., 2014). Furthermore, significant spine loss has been reported in pathological tissue
674 specimens from human epilepsy patients (Multani et al., 1994; Aliashkevich et al., 2003) and
675 in experimental models (Isokawa, 1998; Gibbs et al., 2011). Further, spine loss is directly
676 correlated to the extent of SE induced in animal models and spine number remains altered for
677 weeks (Guo et al., 2012). To verify if miR-135a also regulates spine number, miR-135a was
678 overexpressed in mouse primary hippocampal neurons. Spine density was measured at a
679 distance of 100 µm from the 1$^{st}$ secondary dendritic branch on the apical dendrite (Figure 7C)
680 and 5 different spine types (cup-shaped, mushroom, stubby, thin and filopodium) were
681 counted (Figure 7D). Overexpression of miR-135a led to a significant reduction in the
682 number of spines (0.34 ± 0.13 spines/µm) compared to the control (0.55 ± 0.06 spines/µm).
683 Overexpression of miR-135a *in vitro* caused spine defects that resembled pathological neuron
684 changes observed *in vivo* in TLE. Thus, increased miR-135a expression in epileptic brain
685 could be directly or indirectly contributing to the neuronal spine loss observed. This effect
686 was rescued to control levels when Mef2 vector lacking the 3' UTR was co-expressed with
687 miR-135a (0.49 ± 0.08 spines/µm) (Control vs pre-miR-135a: $t_{(51)} = 5.738$, $p<0.0001$; pre-
688 miR-135a vs pre-miR-135a+Mef2: $t_{(51)} = 4.89$, $p<0.0001$, One-way ANOVA with Sidak *post*
689 *hoc* test; Figure 7E). Interestingly, miR-135a overexpression led to a specific reduction in the
690 number of mature spines: cup-shaped (3.32%), mushroom (18.05%), stubby (20.81%), but
691 led to increase in immature type of spines thin (31.00%) and filopodium (26.82%) compared
692 to control (cup-shaped: 6.60%, mushroom: 34.51%, stubby: 26.53%, thin: 23.16%,
693 filopodium: 9.2%). The reduction in mature spines and increase in immature spine type due

694 to miR-135a overexpression was normalized to control levels when miR-135a was co-
695 expressed with Mef2 (cup-shaped: 5.49%, mushroom: 32.77%, stubby: 25.00%, thin:
696 21.12%, filopodium: 15.63%) (Figure 7F). Thus, increased expression of miR-135a leads to a
697 MEF2-dependent change in spine number and type.

698 Our previous results revealed that miR-135a levels are increased in human and
699 experimental TLE. To examine whether miR-135a and Mef2a could interact in TLE we
700 tested Mef2a expression in mouse and human TLE hippocampus. In line with our model,
701 Mef2a protein expression was significantly reduced in the hippocampus of D14 IAK mice as
702 detected by Western blotting (MWU = 1, p = 0.0317, Mann-whitney U test; Figure 7G-H)
703 and immunohistochemistry (Figure 7I). Similarly, in patients with mTLE, MEF2A expression
704 was strongly reduced in mTLE hippocampal samples compared to controls (MWU = 22.5, p
705 = 0.0316, Mann-whitney U test; Figure 7J-K), and weaker immunostaining was observed in
706 mTLE condition compared to controls in the dentate gyrus and CA region (Figure 7L).
707 Finally, blocking miR-135a *in vivo* using antagomirs resulted in increased Mef2a expression
708 (Figure 7M). Quantification of Mef2a fluorescence intensity in the CA3 region of the
709 hippocampus revealed an increase in Mef2a expression, which as a result of large differences
710 in cell death between animals was not statistically significant (MWU = 51, p = 0.5619,
711 Mann-whitney U test; Figure 7N, O). Together, these results suggest that increased miR-135a
712 expression in hippocampal neurons in mTLE may lead to decreased Mef2a levels. Loss of
713 MEF2 in mTLE could lead to abnormal spine formation and thereby contribute to aberrant
714 firing patterns and cell death observed in epilepsy.
715

716 **Discussion**

717

718 An ever-increasing number of studies implicates altered miRNA expression in epilepsy and
719 identifies these non-coding RNAs as promising therapeutic targets. However, despite this
720 progress, the mechanism-of-action and therapeutic potential of most epilepsy-associated
721 miRNAs remains unknown. Here, we dissected the role of the brain-enriched miRNA miR-
722 135a in TLE. Expression of miR-135a was increased in neurons in human and experimental
723 TLE, particularly during the stage of spontaneous recurrent seizures. Remarkably, silencing
724 miR-135a by intracerebroventricular treatment with antagomirs (ant-135a) during the stage of
725 SRS had potent anti-convulsant effects. These data show that silencing a single miRNA at the
726 SRS stage can rescue mice from spontaneous seizures. To begin to understand how miR-135a
727 deregulation may cause epilepsy and seizures, immunoprecipitation in combination with
728 RNAseq was used to identify miR-135a target RNAs. We report that the activity-dependent
729 transcription factor Mef2a is a neuronal miR-135a target *in vitro* and *in vivo*, that Mef2 is
730 required for miR-135a-induced dendritic spine changes and that miR-135a and Mef2a show
731 reciprocal expression regulation in experimental and human TLE.

732

733 **Targeting spontaneous recurrent seizures with miRNA treatment**

734 miRNAs are emerging as a novel class of therapeutic targets in epilepsy, due to their broad
735 effects on neuronal structure, inflammation, ion channels and gliosis (Cattani et al., 2016;
736 Henshall et al., 2016). Our previous work showed increased expression of miR-135a in
737 human TLE hippocampal samples, an observation subsequently confirmed by others (Kan et
738 al., 2012; Alsharafi and Xiao, 2015). The molecular mechanisms that cause increased miR-
739 135a expression in TLE remain unknown. miR-135a is generated from two different genomic
740 loci in human and mice. Pre-miR-135A2 levels were increased in TLE patients, and both pre-

741 miR-135a1 and pre-miR135a2 were increased in IAK mice, suggesting species-specific gene
742 regulation (Figure 2). Wnt signaling is an attractive candidate for partly explaining this miR-
743 135a regulation, as aberrant Wnt signaling is linked to experimental TLE (Qu et al., 2017)
744 and Wnt signaling is known to control pre-miR-135a expression. For example, during mouse
745 development, canonical Wnt signaling induces the expression of pre-miR-135a2 in dorsal
746 forebrain (Caronia-Brown et al., 2016) and pre-miR-135a2 and its host gene, the long non-
747 coding RNA *RMST*, are induced by Wnt/β-catenin signaling (Anderegg et al., 2013; Caronia-
748 Brown et al., 2016). Several Wnt pathway genes were enriched in the miR-135a bioIP (e.g.
749 Lrp6, Lgr5, Jade1), suggesting an autoregulatory loop between miR-135a and the Wnt
750 pathway in TLE, as reported previously (Anderegg et al., 2013).

751 miRNA antagomirs and mimics have been applied successfully to modulate seizures
752 in experimental TLE (Gross et al., 2016; Henshall et al., 2016). For example, targeting miR-
753 134 before or immediately after SE reduces SRS in multiple animal models of experimental
754 TLE and alters underlying pathological hallmarks (Jimenez-Mateos et al., 2012; Reschke et
755 al., 2017). Further, repeated administration of miR-146a mimics after SE reduces seizures
756 (Iori et al., 2017), while silencing miR-324 delays seizure onset and protects from cell death
757 (Gross et al., 2016). Similarly, targeting miR-203 by antagomirs reduced SRS frequency (Lee
758 et al., 2017). Our study shows that targeting miRNAs at a stage at which SRS have been
759 established, long after SE, also has seizure reducing effects. Antagomirs against miR-135a
760 caused strong reduction of the total number of seizures and average seizure time. Further,
761 treated mice spent less time seizing (Figure 3). In this study, we did not focus on potential
762 long-term disease modifying effects of ant-135a treatment. No neuroprotective effect was
763 found in the first 7 days after ant-135a application (data not shown), but this is in line with
764 the observation that in IAK mice cell death is generally completed in the first week after SE
765 (Mouri et al., 2008). Thus, while further work is needed to establish whether ant-135a

766 treatment has disease-modifying effects, our observation that this treatment has anti-
767 convulsant effects has interesting therapeutic implications as it hints at the possibility of
768 using miRNAs as therapeutic targets after SRS have been established.
769

770 **miR-135a regulates dendritic spines through the epilepsy-associated transcription**
771 **factor Mef2**

772 In the brain, several functions have been reported for miR-135a. It is required for stress
773 resiliency, intact serotonergic activity and has a potential role as an endogenous anti-
774 depressant (Issler et al., 2014). Further, miR-135 is required for sustained spine remodeling
775 and induction of synaptic depression by regulating the SNARE complex proteins Complexin1
776 and 2 (Hu et al., 2014). By targeting Complexin1 and 2, miR-135a regulates synaptic
777 transmission and anxiety-like behavior in the amygdala (Mannironi et al., 2017). Finally,
778 miR-135a induces axon growth and neuronal migration, and axon regeneration after optic
779 nerve injury (van Battum et al., 2018).

780 To begin to understand miR-135a's role in epilepsy and why reducing miR-135a
781 decreases seizure activity, we performed an unbiased biotin-IP screen that revealed several
782 predicted and novel targets of miR-135a (Figure 4). Several of these targets have relevant
783 biological functions and had been implicated in epilepsy, e.g. GR, Mef2a and plexinA4. The
784 glucocorticoid receptor (GR) NR3C1 and Mef2a both regulate neuronal plasticity
785 (Speksnijder et al., 2012) and are deregulated in epilepsy (Huang et al., 2016; Martínez-Levy
786 et al., 2017) Similarly, changes in axon guidance receptors such as PlexinA4, can contribute
787 to mossy fiber sprouting in the dentate gyrus, a critical feature of the epileptic hippocampus
788 leading to hyperexcitability and cell death (Van Battum et al., 2015). The effect of ant-135a
789 treatment on seizure activity was not only strong but also fast, i.e. already after one day
790 significant differences between treated and control mice were found (Figure 3). Explanations

791 for such a swift response are that ant-135a treatment impacts on processes such as synaptic
792 function perhaps through local regulation of gene expression. For example, activity-
793 dependent local translation regulation of target mRNAs by miRNAs occurs in single
794 synapses (Sambandan et al., 2017). Therefore, loss of miR-135a may lead to de-repression of
795 its target mRNAs in distal dendrites leading to changes in excitatory neurotransmission
796 observed in epileptic networks (McNamara et al., 2006). Interestingly, one of the targets of
797 miR-135a that we identified was Mef2a, an activity-dependent transcription factor that
798 regulates excitatory and inhibitory synaptic strength both locally at synapses and in the
799 nucleus (Flavell et al., 2008). Overexpression of miR-135a in cultured mouse hippocampal
800 neurons reduced spine number and increased the relative number of immature spines, in line
801 with the profound loss of dendritic spines found in epilepsy (Swann et al., 2000). Both
802 defects were rescued by re-expression of miR-135a-insensitive Mef2, implicating a miR-
803 135a-Mef2 pathway in the control of spine maturation and number (Figure 7). This together
804 with the observation that miR-135a and Mef2a show reciprocal expression regulation in TLE
805 invites the speculation that miR-135a may regulate Mef2a to induce synaptic defects in TLE.

806 Mef2 proteins function as synapse eliminating factors in development and disease
807 (Pfeiffer et al., 2010; Tsai et al., 2012; Wang, 2016), but can also regulate genes known to
808 mediate synapse weakening (e.g. Homer1a, Arc, kcna1) or strengthening (e.g. leucine-rich
809 glioma-inactivated 1 (Lgi1), BDNF, adenyl cylase 8) (Flavell et al., 2008). Several of these
810 genes have been implicated in epilepsy. For example, loss of Lgi1 in glutamatergic neurons
811 induces epileptic seizures due to increased synaptic glutamate levels leading to
812 hyperexcitable neuronal networks (Boillot et al., 2014, 2016). In addition, BDNF has a dual
813 role, as a pro-epileptic and anti-epileptogenic factor (Simonato et al., 2006). BDNF
814 expression is increased immediately after SE but reduced during the chronic stage. It
815 selectively localizes to dendritic compartments after chemoconvulsant seizures (Tongiorgi,

816 2004). A recent study shows that continuous release of BDNF into the epileptic hippocampus
817 reduces the frequency of generalized seizures and rescues from histological alterations
818 observed in chronic epilepsy (Falcicchia et al., 2018). Further work is needed to explore
819 whether the morphological and seizure-suppressive effects of ant-135 derive from effects on
820 these or other Mef2 targets, and whether these effects originate from altered functioning of
821 glutamatergic synapses (e.g. Lgi1) or of both glutamatergic and GABAergic synapses (e.g.
822 BDNF) (Simonato et al., 2006; Gu et al., 2017). *Mef2c* knockout mice show a reduction in
823 excitatory synapse number but an increase in inhibitory synapse number. It has therefore
824 been proposed that Mef2c simultaneously regulates spine density on both inhibitory and
825 excitatory neurons to maintain balanced activity in neuronal networks (Harrington et al.,
826 2016). Disruption of this regulation may lead to abnormal synaptic activity leading to seizure
827 activity in TLE.
828
829 In conclusion, a deeper understanding of the roles, targets and mechanisms-of-action of
830 miRNAs in the pathogenesis of epilepsy may lead to the development of novel diagnostic
831 biomarkers and the identification of therapeutic targets for treatment. Here, we identify miR-
832 135a as a target for reducing SRS once these seizures have already been established. This is
833 important as the majority of studies so far have focused on miRNA manipulation during or at
834 least starting in the acute stages of the disease. It will be interesting to explore whether
835 manipulation of other miRNAs at the SRS stage also has seizure-suppressive effects or even
836 disease-modifying properties. Further insight into how miR-135a expression is regulated in
837 epilepsy and which miR-135a targets, in addition to Mef2a, are affected by ant-135a
838 administration in experimental epilepsy will provide more insight into the mechanism-of-
839 action of miR-135a in TLE.

840 **References**

841

842 Aliashkevich AF, Yilmazer-Hanke D, Van Roost D, Mundhenk B, Schramm J, Blümcke I
843 (2003) Cellular pathology of amygdala neurons in human temporal lobe epilepsy. Acta
844 Neuropathol 106:99–106.
845 Alsharafi W, Xiao B (2015) Dynamic Expression of MicroRNAs (183, 135a, 125b, 128, 30c
846 and 27a) in the Rat Pilocarpine Model and Temporal Lobe Epilepsy Patients. CNS
847 Neurol Disord - Drug Targets.
848 Anderegg A, Lin HP, Chen JA, Caronia-Brown G, Cherepanova N, Yun B, Joksimovic M,
849 Rock J, Harfe BD, Johnson R, Awatramani R (2013) An Lmx1b-miR135a2 Regulatory
850 Circuit Modulates Wnt1/Wnt Signaling and Determines the Size of the Midbrain
851 Dopaminergic Progenitor Pool. PLoS Genet 9.
852 Anders S, Pyl PT, Huber W (2015) HTSeq-A Python framework to work with high-
853 throughput sequencing data. Bioinformatics 31:166–169.
854 Aronica E, Fluiter K, Iyer a, Zurolo E, Vreijling J, van Vliet E a, Baayen JC, Gorter J a
855 (2010) Expression pattern of miR-146a, an inflammation-associated microRNA, in
856 experimental and human temporal lobe epilepsy. Eur J Neurosci 31:1100–1107.
857 Bartel DP (2018) Metazoan MicroRNAs. Cell 173:20–51 Available at:
858 https://doi.org/10.1016/j.cell.2018.03.006.
859 Becker AJ, Chen J, Zien A, Sochivko D, Normann S, Schramm J, Elger CE, Wiestler OD,
860 Blümcke I (2003) Correlated stage- and subfield-associated hippocampal gene
861 expression patterns in experimental and human temporal lobe epilepsy. Eur J Neurosci
862 18:2792–2802 Available at:
863 http://www3.interscience.wiley.com/journal/118846300/abstract.
864 Bienvenu T, Diebold B, Chelly J, Isidor B (2013) Refining the phenotype associated with

865 MEF2C point mutations. Neurogenetics 14:71–75.

866 Blümcke I et al. (2013) International consensus classification of hippocampal sclerosis in
867 temporal lobe epilepsy: A Task Force report from the ILAE Commission on Diagnostic
868 Methods. Epilepsia.

869 Boillot M, Huneau C, Marsan E, Lehongre K, Navarro V, Ishida S, Dufresnois B, Ozkaynak
870 E, Garrigue J, Miles R, Martin B, Leguern E, Anderson MP, Baulac S (2014)
871 Glutamatergic neuron-targeted loss of LGI1 epilepsy gene results in seizures. Brain
872 137:2984–2996.

873 Boillot M, Lee CY, Allene C, Leguern E, Baulac S, Rouach N (2016) LGI1 acts
874 presynaptically to regulate excitatory synaptic transmission during early postnatal
875 development. Sci Rep 6:1–9 Available at: http://dx.doi.org/10.1038/srep21769.

876 Brennecke J, Stark A, Russell RB, Cohen SM (2005) Principles of microRNA-target
877 recognition. PLoS Biol 3:0404–0418.

878 Caronia-Brown G, Anderegg A, Awatramani R (2016) Expression and functional analysis of
879 the Wnt/beta-catenin induced mir-135a-2 locus in embryonic forebrain development.
880 Neural Dev 11:1–15 Available at: http://dx.doi.org/10.1186/s13064-016-0065-y.

881 Cattani AA, Allene C, Seifert V, Rosenow F, Henshall DC, Freiman TM (2016) Involvement
882 of microRNAs in epileptogenesis. Epilepsia 57:1015–1026.

883 Chang BS, Lowenstein DH (2003) Epilepsy. N Engl J Med.

884 Dang Z, Xu WH, Lu P, Wu N, Liu J, Ruan B, Zhou L, Song WJ, Dou KF (2014) MicroRNA-
885 135a inhibits cell proliferation by targeting Bmi1 in pancreatic ductal adenocarcinoma.
886 Int J Biol Sci 10:733–745.

887 Ebert MS, Sharp P a. (2012) Roles for MicroRNAs in conferring robustness to biological
888 processes. Cell 149:505–524 Available at: http://dx.doi.org/10.1016/j.cell.2012.04.005.

889 Engel J (2001) A proposed diagnostic scheme for people with epileptic seizures and with

890 epilepsy: Report of the ILAE task force on classification and terminology. Epilepsia.

891 Falcicchia C, Paolone G, Emerich DF, Lovisari F, Bell WJ, Fradet T, Wahlberg LU,
892 Simonato M (2018) Seizure-Suppressant and Neuroprotective Effects of Encapsulated
893 BDNF-Producing Cells in a Rat Model of Temporal Lobe Epilepsy. Mol Ther - Methods
894 Clin Dev 9:211–224 Available at:
895 https://www.sciencedirect.com/science/article/pii/S2329050118300251.

896 Fiore R, Khudayberdiev S, Christensen M, Siegel G, Flavell SW, Kim T-K, Greenberg ME,
897 Schratt G (2009) Mef2-mediated transcription of the miR379-410 cluster regulates
898 activity-dependent dendritogenesis by fine-tuning Pumilio2 protein levels. EMBO J
899 28:697–710.

900 Flavell SW, Cowan CW, Kim T-K, Greer PL, Lin Y, Paradis S, Griffith EC, Hu LS, Chen C,
901 Greenberg ME (2006) Activity-dependent regulation of MEF2 transcription factors
902 suppresses excitatory synapse number. Science 311:1008–1012.

903 Flavell SW, Kim T-K, Gray JM, Harmin D a, Hemberg M, Hong EJ, Markenscoff-
904 Papadimitriou E, Bear DM, Greenberg ME (2008) Genome-wide analysis of MEF2
905 transcriptional program reveals synaptic target genes and neuronal activity-dependent
906 polyadenylation site selection. Neuron 60:1022–1038 Available at:
907 http://www.pubmedcentral.nih.gov/articlerender.fcgi?artid=2630178&tool=pmcentrez&
908 rendertype=abstract [Accessed February 28, 2013].

909 Gibbs S, Chattopadhyaya B, Desgent S, Awad PN, Clerk-Lamalice O, Levesque M, Vianna
910 RM, Rébillard RM, Delsemme AA, Hébert D, Tremblay L, Lepage M, Descarries L, Di
911 Cristo G, Carmant L (2011) Long-term consequences of a prolonged febrile seizure in a
912 dual pathology model. Neurobiol Dis 43:312–321 Available at:
913 http://dx.doi.org/10.1016/j.nbd.2011.02.013.

914 Gorter J a., Iyer A, White I, Colzi A, van Vliet E a., Sisodiya S, Aronica E (2014)

915 Hippocampal subregion-specific microRNA expression during epileptogenesis in
916 experimental temporal lobe epilepsy. Neurobiol Dis 62:508–520 Available at:
917 http://dx.doi.org/10.1016/j.nbd.2013.10.026.
918 Gross C, Yao X, Engel T, Tiwari D, Xing L, Rowley S, Danielson SW, Thomas KT,
919 Jimenez-Mateos EM, Schroeder LM, Pun RYK, Danzer SC, Henshall DC, Bassell GJ
920 (2016) MicroRNA-Mediated Downregulation of the Potassium Channel Kv4.2
921 Contributes to Seizure Onset. Cell Rep 17:37–45 Available at:
922 http://dx.doi.org/10.1016/j.celrep.2016.08.074.
923 Gu F, Parada I, Shen F, Li J, Bacci A, Graber K, Taghavi RM, Scalise K, Schwartzkroin P,
924 Wenzel J, Prince DA (2017) Structural alterations in fast-spiking GABAergic
925 interneurons in a model of posttraumatic neocortical epileptogenesis. Neurobiol Dis
926 108:100–114 Available at: http://dx.doi.org/10.1016/j.nbd.2017.08.008.
927 Guo D, Arnspiger S, Rensing NR, Wong M (2012) Brief seizures cause dendritic injury.
928 Neurobiol Dis 45:348–355.
929 Harrington AJ, Raissi A, Rajkovich K, Berto S, Kumar J, Molinaro G, Raduazzo J, Guo Y,
930 Loerwald K, Konopka G, Huber KM, Cowan CW (2016) MEF2C regulates cortical
931 inhibitory and excitatory synapses and behaviors relevant to neurodevelopmental
932 disorders. Elife 5:1–27.
933 Henshall DC, Hamer HM, Pasterkamp RJ, Goldstein DB, Kjems J, Prehn JHM, Schorge S,
934 Lamottke K, Rosenow F (2016) MicroRNAs in epilepsy: pathophysiology and clinical
935 utility. Lancet Neurol 15:1368–1376 Available at: http://dx.doi.org/10.1016/S1474-
936 4422(16)30246-0.
937 Höck J, Meister G (2008) The Argonaute protein family. Genome Biol 9.
938 Hu Z, Yu D, Gu Q, Yang Y, Tu K, Zhu J, Li Z (2014) miR-191 and miR-135 are required for
939 long-lasting spine remodelling associated with synaptic long-term depression. Nat

940 Commun 5:3263 Available at: http://www.ncbi.nlm.nih.gov/pubmed/24535612.
941 Huang Y, Wu X, Guo J, Yuan J (2016) Myocyte-specific enhancer binding factor 2A
942 expression is downregulated during temporal lobe epilepsy. Int J Neurosci 126:786–796.
943 Iori V, Iyer AM, Ravizza T, Beltrame L, Paracchini L, Marchini S, Cerovic M, Hill C, Ferrari
944 M, Zucchetti M, Molteni M, Rossetti C, Brambilla R, Steve White H, D'Incalci M,
945 Aronica E, Vezzani A (2017) Blockade of the IL-1R1/TLR4 pathway mediates disease-
946 modification therapeutic effects in a model of acquired epilepsy. Neurobiol Dis 99:12–
947 23 Available at: http://dx.doi.org/10.1016/j.nbd.2016.12.007.
948 Isokawa M (1998) Remodeling dendritic spines in the rat pilocarpine model of temporal lobe
949 epilepsy. Neurosci Lett 258:73–76.
950 Issler O, Haramati S, Paul ED, Maeno H, Navon I, Zwang R, Gil S, Mayberg HS, Dunlop
951 BW, Menke A, Awatramani R, Binder EB, Deneris ES, Lowry C a., Chen A (2014)
952 MicroRNA 135 is essential for chronic stress resiliency, antidepressant efficacy, and
953 intact serotonergic activity. Neuron 83:344–360 Available at:
954 http://dx.doi.org/10.1016/j.neuron.2014.05.042.
955 Jimenez-Mateos EM, Engel T, Merino-Serrais P, McKiernan RC, Tanaka K, Mouri G, Sano
956 T, O'Tuathaigh C, Waddington JL, Prenter S, Delanty N, Farrell M a, O'Brien DF,
957 Conroy RM, Stallings RL, DeFelipe J, Henshall DC (2012) Silencing microRNA-134
958 produces neuroprotective and prolonged seizure-suppressive effects. Nat Med 18:1087–
959 1094.
960 Jimenez-Mateos EM, Henshall DC (2013) Epilepsy and microRNA. Neuroscience 238:218–
961 229 Available at: http://dx.doi.org/10.1016/j.neuroscience.2013.02.027.
962 Kan AA, Van Erp S, Derijck AAHA, De Wit M, Hessel EVS, O'Duibhir E, De Jager W, Van
963 Rijen PC, Gosselaar PH, De Graan PNE, Pasterkamp RJ (2012) Genome-wide
964 microRNA profiling of human temporal lobe epilepsy identifies modulators of the

965 immune response. Cell Mol Life Sci 69:3127–3145.

966 Kosik KS (2006) The neuronal microRNA system. Nat Rev Neurosci 7:911–920.

967 Krek A, Grün D, Poy MN, Wolf R, Rosenberg L, Epstein EJ, MacMenamin P, Da Piedade I,
968 Gunsalus KC, Stoffel M, Rajewsky N (2005) Combinatorial microRNA target
969 predictions. Nat Genet 37:495–500.

970 Lee ST, Jeon D, Chu K, Jung KH, Moon J, Sunwoo J, Park DK, Yang H, Park JH, Kim M,
971 Roh JK, Lee SK (2017) Inhibition of miR-203 Reduces Spontaneous Recurrent Seizures
972 in Mice. Mol Neurobiol 54:3300–3308.

973 Lewis BP, Burge CB, Bartel DP (2005) Conserved seed pairing, often flanked by adenosines,
974 indicates that thousands of human genes are microRNA targets. Cell 120:15–20.

975 Löscher W, Klitgaard H, Twyman RE, Schmidt D (2013) New avenues for anti-epileptic
976 drug discovery and development. Nat Rev Drug Discov 12:757–776 Available at:
977 http://dx.doi.org/10.1038/nrd4126.

978 Lyons GE, Micales BK, Schwarz J, Martin JF, Olson EN (1995) Expression of mef2 genes in
979 the mouse central nervous system suggests a role in neuronal maturation. J Neurosci
980 15:5727–5738 Available at: http://www.ncbi.nlm.nih.gov/pubmed/7643214.

981 Mannironi C, Biundo A, Rajendran S, De Vito F, Saba L, Caioli S, Zona C, Ciotti T, Caristi
982 S, Perlas E, Del Vecchio G, Bozzoni I, Rinaldi A, Mele A, Presutti C (2017) miR-135a
983 Regulates Synaptic Transmission and Anxiety-Like Behavior in Amygdala. Mol
984 Neurobiol 55:3301–3315.

985 Martínez-Levy GA, Rocha L, Rodríguez-Pineda F, Alonso-Vanegas MA, Nani A, Buentello-
986 García RM, Briones-Velasco M, San-Juan D, Cienfuegos J, Cruz-Fuentes CS (2017)
987 Increased Expression of Brain-Derived Neurotrophic Factor Transcripts I and VI, cAMP
988 Response Element Binding, and Glucocorticoid Receptor in the Cortex of Patients with
989 Temporal Lobe Epilepsy. Mol Neurobiol:1–11.

990 McNamara JO, Huang YZ, Leonard a S (2006) Molecular signaling mechanisms underlying
991 epileptogenesis. Sci STKE 2006:re12.
992 Moshé SL, Perucca E, Ryvlin P, Tomson T (2015) Epilepsy: New advances. Lancet 385:884–
993 898.
994 Mouri G, Jimenez-Mateos E, Engel T, Dunleavy M, Hatazaki S, Paucard A, Matsushima S,
995 Taki W, Henshall DC (2008) Unilateral hippocampal CA3-predominant damage and
996 short latency epileptogenesis after intra-amygdala microinjection of kainic acid in mice.
997 Brain Res 1213:140–151.
998 Multani P, Myers RH, Blume HW, Schomer DL, Sotrel A (1994) Neocortical Dendritic
999 Pathology in Human Partial Epilepsy: A Quantitative Golgi Study. Epilepsia.
1000 Nowakowska BA, Obersztyn E, Szymańska K, Bekiesińska-Figatowska M, Xia Z, Ricks CB,
1001 Bocian E, Stockton DW, Szczałuba K, Nawara M, Patel A, Scott DA, Cheung SW,
1002 Bohan TP, Stankiewicz P (2010) Severe mental retardation, seizures, and hypotonia due
1003 to deletions of MEF2C. Am J Med Genet Part B Neuropsychiatr Genet 153:1042–1051.
1004 Ørom UA, Lund AH (2007) Isolation of microRNA targets using biotinylated synthetic
1005 microRNAs. Methods 43:162–165.
1006 Ørom UA, Nielsen FC, Lund AH (2008) MicroRNA-10a Binds the 5′UTR of Ribosomal
1007 Protein mRNAs and Enhances Their Translation. Mol Cell 30:460–471.
1008 Pfeiffer BE, Zang T, Wilkerson JR, Taniguchi M, Maksimova M a, Smith LN, Cowan CW,
1009 Huber KM (2010) Fragile X mental retardation protein is required for synapse
1010 elimination by the activity-dependent transcription factor MEF2. Neuron 66:191–197
1011 Available at:
1012 http://www.pubmedcentral.nih.gov/articlerender.fcgi?artid=2864778&tool=pmcentrez&
1013 rendertype=abstract [Accessed March 9, 2013].
1014 Qu Z, Su F, Qi X, Sun J, Wang H, Qiao Z, Zhao H, Zhu Y (2017) Wnt/beta-catenin

1015 signalling pathway mediated aberrant hippocampal neurogenesis in kainic acid-induced
1016 epilepsy. Cell Biochem.
1017 Rakhade SN, Jensen FE (2009) Epileptogenesis in the immature brain: Emerging
1018 mechanisms. Nat Rev Neurol.
1019 Reschke CR, Silva LFA, Norwood BA, Senthilkumar K, Morris G, Sanz-Rodriguez A,
1020 Conroy RM, Costard L, Neubert V, Bauer S, Farrell MA, O'Brien DF, Delanty N,
1021 Schorge S, Pasterkamp RJ, Rosenow F, Henshall DC (2017) Potent Anti-seizure Effects
1022 of Locked Nucleic Acid Antagomirs Targeting miR-134 in Multiple Mouse and Rat
1023 Models of Epilepsy. Mol Ther - Nucleic Acids 6:45–56 Available at:
1024 http://dx.doi.org/10.1016/j.omtn.2016.11.002.
1025 Robinson M, McCarthy D, Smyth G (2010) edgeR: a Bioconductor package for differential
1026 expression analysis of digital gene expression data. Bioinformatics.
1027 Robinson MD, Oshlack A (2010) A scaling normalization method for differential expression
1028 analysis of RNA-seq data. Genome Biol.
1029 Sambandan S, Akbalik G, Kochen L, Rinne J, Kahlstatt J, Glock C, Tushev G, Alvarez-
1030 Castelao B, Heckel A, Schuman EM (2017) Activity-dependent spatially localized
1031 miRNA maturation in neuronal dendrites. Science (80- ) 355:634–637.
1032 Semah F, Picot MC, Adam C, Broglin D, Arzimanoglou A, Bazin B, Cavalcanti D, Baulac M
1033 (1998) Is the underlying cause of epilepsy a major prognostic factor for recurrence?
1034 Neurology.
1035 Simonato M, Tongiorgi E, Kokaia M (2006) Angels and demons: neurotrophic factors and
1036 epilepsy. Trends Pharmacol Sci 27:631–638.
1037 Speksnijder N, Christensen K V., Didriksen M, De Kloet ER, Datson NA (2012)
1038 Glucocorticoid receptor and myocyte enhancer factor 2 cooperate to regulate the
1039 expression of c-JUN in a neuronal context. J Mol Neurosci 48:209–218.

1040 Staley K (2004) Epileptic Neurons Go Wireless. 1538:1–30.

1041 Supek F, Bošnjak M, Škunca N, Šmuc T (2011) Revigo summarizes and visualizes long lists
1042 of gene ontology terms. PLoS One 6.

1043 Swann JW, Al-Noori S, Jiang M, Lee CL (2000) Spine loss and other dendritic abnormalities
1044 in epilepsy. Hippocampus 10:617–625.

1045 Tongiorgi E (2004) Brain-Derived Neurotrophic Factor mRNA and Protein Are Targeted to
1046 Discrete Dendritic Laminas by Events That Trigger Epileptogenesis. J Neurosci
1047 24:6842–6852 Available at:
1048 http://www.jneurosci.org/cgi/doi/10.1523/JNEUROSCI.5471-03.2004.

1049 Tsai N-P, Wilkerson JR, Guo W, Maksimova M a, DeMartino GN, Cowan CW, Huber KM
1050 (2012) Multiple autism-linked genes mediate synapse elimination via proteasomal
1051 degradation of a synaptic scaffold PSD-95. Cell 151:1581–1594 Available at:
1052 http://www.ncbi.nlm.nih.gov/pubmed/23260144 [Accessed March 3, 2013].

1053 Van Battum EY, Brignani S, Pasterkamp RJ (2015) Axon guidance proteins in neurological
1054 disorders. Lancet Neurol 14:532–546 Available at: http://dx.doi.org/10.1016/S1474-
1055 4422(14)70257-1.

1056 Van Battum EY, Gunput RAF, Lemstra S, Groen EJN, Yu K Lou, Adolfs Y, Zhou Y,
1057 Hoogenraad CC, Yoshida Y, Schachner M, Akhmanova A, Pasterkamp RJ (2014) The
1058 intracellular redox protein MICAL-1 regulates the development of hippocampal mossy
1059 fibre connections. Nat Commun 5.

1060 van Battum EY, Verhagen MG, Vangoor VR, Fujita Y, Derijck AAHA, O'Duibhir E,
1061 Giuliani G, de Gunst T, Adolfs Y, Lelieveld D, Egan D, Schaapveld RQJ, Yamashita T,
1062 Pasterkamp RJ (2018) An Image-Based miRNA screen identifies miRNA-135s as
1063 regulators of CNS axon growth and regeneration by targeting Krüppel-like factor 4. J
1064 Neurosci:0662-17 Available at:

1065 http://www.jneurosci.org/lookup/doi/10.1523/JNEUROSCI.0662-17.2017.
1066 Wang J (2016) Myocyte Enhancer Factor-2 (MEF2) in Diseases of Central Nervous System:
1067 A Mini Review. Explor Res Hypothesis Med 1:4–8 Available at:
1068 http://www.xiahepublishing.com/ArticleFullText.aspx?sid=2&jid=2&id=10.14218%2F
1069 ERHM.2015.00001.
1070 Wani S, Cloonan N (2014) Profiling direct mRNA-microRNA interactions using synthetic
1071 biotinylated microRNA-duplexes. bioRxiv.
1072 Wetherington J, Serrano G, Dingledine R (2008) Astrocytes in the Epileptic Brain. Neuron
1073 58:168–178.
1074 Wieser H-G (2004) ILAE Commission Report. Mesial temporal lobe epilepsy with
1075 hippocampal sclerosis. Epilepsia.
1076 Xiang H, Zhong ZX, Peng YD, Jiang SW (2017) The emerging role of Zfp217 in
1077 adipogenesis. Int J Mol Sci 18:1–17.
1078 Young MD, Wakefield MJ, Smyth GK, Oshlack A (2010) Gene ontology analysis for RNA-
1079 seq: accounting for selection bias. Genome Biol.
1080 Zhao X, Sun Z, Li H, Jiang F, Zhou J, Zhang L (2017) MiR-135a-5p modulates biological
1081 functions of thyroid carcinoma cells via targeting VCAN 3′-UTR. Cancer Biomarkers.
1082 Zhou W, Li X, Liu F, Xiao Z, He M, Shen S, Liu S (2012) MiR-135a promotes growth and
1083 invasion of colorectal cancer via metastasis suppressor 1 in vitro. Acta Biochim Biophys
1084 Sin 44:838–846.
1085
1086
1087
1088
1089

1090 **Figure legends**

1091

1092 **Figure 1**: **Increased miR-135a expression in human TLE**.

1093 A) Expression levels of miR-135a in human TLE patients determined by quantitative PCR.
1094 Controls (n=8), mTLE (n=7). Normalized to 5s rRNA. Data is expressed as mean ± SEM,
1095 **p<0.01. t test. B) LNA *in situ* hybridization showing localization of miR-135a in control
1096 and mTLE groups. Scale bar, 200 μm. C) Cell-type specific localization of miR-135a. Co-
1097 localization with neuronal marker, NeuN. Specific localization of miR-135a was observed in
1098 neuronal soma in the CA regions. Arrows indicate co-labelled cells. No co-localization with
1099 the astrocytic marker Glial fibrillary acidic protein (GFAP) was observed. Scale bar, 25 μm.

1100

1101 **Figure 2**: **Increased miR-135a in a mouse model of TLE**.

1102 A) Increased miR-135a levels in the hippocampus of IAK mice 2 weeks after SE. n=4 PBS
1103 and n=3 IAK mice. Normalized to 5s rRNA. Data is expressed as mean ± SEM. *p<0.05. t
1104 test. B) Representative images of *in situ* hybridization (ISH) showing strong miR-135a
1105 expression in hippocampus and amygdala regions at 2 weeks after SE induction compared to
1106 24 h and PBS injections. Scramble stained images were devoid of signal. CTX, cortex; HC,
1107 hippocampus; TH, thalamus; Amyg, amygdala. Scale bar, 300 μm. C) Fluorescent ISH for
1108 miR-135a in combination with immunohistochemistry for the astrocytic marker GFAP and
1109 neuronal marker NeuN. miR-135a showed no specific co-localization with GFAP. Dentate
1110 gyrus PML, polymorph layer; ML, molecular layer; GCL, granule cell layer; CA, cornu
1111 ammonis region. Scale bar, 100 μm. D) Genomic location and sequence of miR-135a in
1112 human and mice. Mature miR-135a-5p is spliced from two pre-sequences in mice and human.
1113 E) Increased levels of miR-135A-2 in mTLE condition but no change in miR-135A-1. n=8
1114 controls and n=7 mTLE samples. Data is expressed as mean ± SEM, *p<0.05. *t* test. F) Both

1115 miR-135a-1 and miR-135a-2 levels are increased in IAK mice compared to PBS injected
1116 controls. n=4 PBS and n=3 KA mice. Data is expressed as mean ± SEM, ***p<0.001,
1117 *p<0.05. *t* test.
1118
1119 **Figure 3: Ant-135a reduces seizures in the mouse intra-amygdala kainate model of**
1120 **epilepsy.**
1121 A) miR-135a expression levels 24 h after administration of ant-135a. Significant reduction of
1122 miR-135a levels at 1.0, 1.5 nmol compared to vehicle injection. No off-target effect observed
1123 at 1.0 nmol, but reduction in miR-124 levels was observed at 1.5 nmol. Normalized to
1124 RNU6B. Data is expressed as mean ± SEM, *p<0.05, One-way ANOVA with Sidak *post hoc*
1125 test. **B)** LNA *in situ* hybridization (ISH) for the miR-135a inhibitor probe in ant-135a injected
1126 mice. Strong signal for ant-135a is observed in ipsilateral (injected) hippocampus (images 1,
1127 2) while the control is devoid of specific signal. Scale bar, 200 μm. Ant-135a is taken up by
1128 neurons in hippocampal CA1, CA4 and DG regions. Scale bar, 50 μm. **C)** Male C57BL6
1129 adult mice (~25g) were implanted with DSI telemetry devices connected to cortical
1130 electrodes (both brain hemispheres) for EEG recordings. After appropriate surgical recovery
1131 mice were connected to the EEG equipment, and underwent intra-amygdala kainic acid-
1132 induced status epilepticus (SE) on Day Zero (D0). Telemetry devices were turned off and
1133 reactivated on Day 7 (D07) to record a 7-days "**Epileptic Baseline"**. On Day 14 (D14) mice
1134 were intracerebroventricularly (i.c.v) injected with ant-135a or its scramble control, and
1135 continuously monitored for 7 days (D14 to D21; "**after antagomir treatement period"**).
1136 **D)** Graph shows the total number of SRS per day per mouse. **Epileptic baseline**: No
1137 significant difference was detected between treated and control animals in seizure frequency
1138 during the 7 days of epileptic baseline (p=0.743). **After antagomir treatment**: Following
1139 treatment (on D14), a strong decrease in the number of seizures was detected in the

1140 antagomir treated group starting from D15. **E)** Seizure count is represented as mean and SD
1141 over the EEG recording period. Application of ant-135a at day 14 (dotted line) resulted in a
1142 significant decrease in seizure count with respect to time. n=5 for control and ant-135a.
1143 ***p<0.001, mixed design repeated measures general linear model; day/treatment interaction.
1144 **F)** Average seizure duration: **Epileptic baseline**: No significant difference between treated
1145 and control animals in seizure duration during the 7 days of epileptic baseline (p=0·4721).
1146 **After antagomir treatment**: Following treatment (on D14), ant-135a-treated mice presented
1147 significantly shorter seizures than the control group, n=5 mice per group, ***p<0.001, t test.
1148 **G) Time spent in ictal activity: Epileptic baseline**: No significant difference between
1149 treated and control animals in total time spent in seizures during the 7 days of epileptic
1150 baseline (p=0·7546). **After antagomir treatment**: Following treatment (on D14), ant-135a-
1151 treated mice spent significantly less time in seizures than control mice. n=5 mice per group,
1152 **p<0.01, t test. **H)** Representative EEG traces of spontaneous seizures 3 days after treatment
1153 with ant-135a (bottom) or control (top). **I)** Total time spent in seizures. Diagram illustrates
1154 seizure burden per day (seconds) per mouse before and after the antagomir treatment (dotted
1155 line). A control mouse with high number of seizures died on day 7 after antagomir treatment
1156 period.
1157
1158 **Figure 4: Target identification for miR-135a using biotinylated probes.**
1159 A) Schematic of miRNA duplex design. The mature strand is labelled with a biotin molecule
1160 at the 3' hydroxyl group via a C6 linker. B) Schematic showing the immunoprecipitation (IP)
1161 procedure. Neuro2A cells were transfected with biotin tagged probes, IP was performed
1162 using Streptavidin beads. Total RNA was extracted and subjected to deep RNA sequencing.
1163 n=3 biological replicates/ group. C) Representative western blot for Ago2 in miR-135a and
1164 negative control IP samples. β-actin was used as a loading control and only present in input

1165 samples. No tr: no transfection control, NC – negative control, In – inputs, IP –
1166 immunoprecipitates. D) Heat maps of RNA from input and IP samples showing differential
1167 gene expression. E) Principal component analysis (PCA) plots of inputs and IPs showing the
1168 clustering of samples basing on their differential gene expression. NCIP – negative control
1169 IP, AIP – miR-135a IP.
1170
1171 **Figure 5: Gene Ontology analysis of miR-135a targets.**
1172 A-C) Gene Ontology terms for miRNA bioIPs highlighting various processes that could
1173 potentially be regulated by miR-135a. D) Venn diagram showing the overlap of predicted
1174 binding sequence location (targeting site for miR-135a) in various segments of a transcript.
1175 E) Venn diagram showing the common (50.4%) and unique targets of miR-135a and
1176 miR135b. miR-135a and miR-135b contain the same mature sequence with only one mis-
1177 match outside the seed region.
1178
1179 **Figure 6: Validation of bio-IP targets.**
1180 A) Several of the selected targets were tested by qPCR and were significantly enriched in the
1181 IP samples compared to inputs. Bar graphs and representative blot images showing
1182 Glucocorticoid Receptor (B-B1), PlexinA4 (C-C1) and Mef2a (D-D1) protein levels
1183 normalized to β-actin after miR-135a overexpression in N2A cells. All of the validated
1184 targets were significantly downregulated after miR-135a overexpression compared to
1185 negative control (NC) condition. Data is expressed as means, mean ± SEM, *$p<0.05$, *t* test.
1186
1187 **Figure 7: MiR-135a regulates dendritic spines through Mef2a and Mef2a is deregulated**
1188 **in TLE.**

1189 A) Schematic representation of the 3' UTR of Mef2a with the miR-135a target site. B) miR-
1190 135a target site was ligated into the psiCheck2 vector and used in the Renilla-luciferase
1191 assay. Luciferase assay in Hek293 cells transfected with the constructs carrying miR-135a
1192 WT and mutant binding sites, co-transfected with and without miR-135a mimic. n=2
1193 independent experiments were performed with 4 wells/condition each time. Data is expressed
1194 as mean ± SEM, **p<0.01. *t* test. NC- negative control. C) Representative image showing
1195 secondary apical dendrites quantified for spine density. Dissociated neurons were transfected
1196 with miR-135a (with or without Mef2) or control vectors at DIV13 and fixed and analyzed at
1197 DIV17. D) Schematic showing the different types of spines quantified. E) Histogram
1198 showing the quantification of spine number. Reduced spine density is observed after miR-
1199 135a overexpression and this effect is rescued by co-transfection with Mef2. n=12-22
1200 neurons were analyzed from three independent transfections. Data is expressed as mean ±
1201 SEM. ****p<0.0001, One-way ANOVA with Sidak *post hoc* test. F) Graph showing the
1202 percentage of different spine types. An increase in immature spines is observed after miR-
1203 135a overexpression, which is rescued after Mef2 co-expression. G) Representative Western
1204 blot of Mef2a of hippocampal tissue of control and IAK mice at 2 weeks after SE. Mef2a is
1205 strongly reduced in experimental mice. H) Quantification of total protein levels normalized to
1206 β-actin. n=5 controls, n=4 KA mouse hippocampi. Data is expressed as mean ± SEM.
1207 *p<0.05. Mann-whitney U test. I) Representative image of Mef2a immunostaining in
1208 hippocampal subregions of IAK mice. Scale bar, 100 μm. J) Representative Western blot of
1209 Mef2a in hippocampi of control and mTLE+HS patients. K) Quantification of total protein
1210 levels normalized to β-actin. n=6 controls, n=4 mTLE+HS. Data is expressed as mean ±
1211 SEM. *p<0.05. Mann-whitney U test. L) Representative image of Mef2a immunostaining in
1212 controls and mTLE+HS dentate gyrus (DG) and CA regions. Arrows indicate CA neurons
1213 that are devoid of Mef2a expression. Scale 50 μm. M) Mef2a immunostaining in PBS control

1214 and ant-135a injected mice. Dotted insets showing the region used for quantification. Scale
1215 bar, 200 μm. N) Representative region of interest (ROI) from CA3 images used for
1216 quantifying Mef2a intensity. Mice1 (1), Mice2 (2). Scale bar, 25 μm. O) Mef2a fluorescence
1217 intensity in Ant-135a and control mice. n=3 controls and n=3 Ant-135a mice. Mean ratio
1218 between conditions is shown.

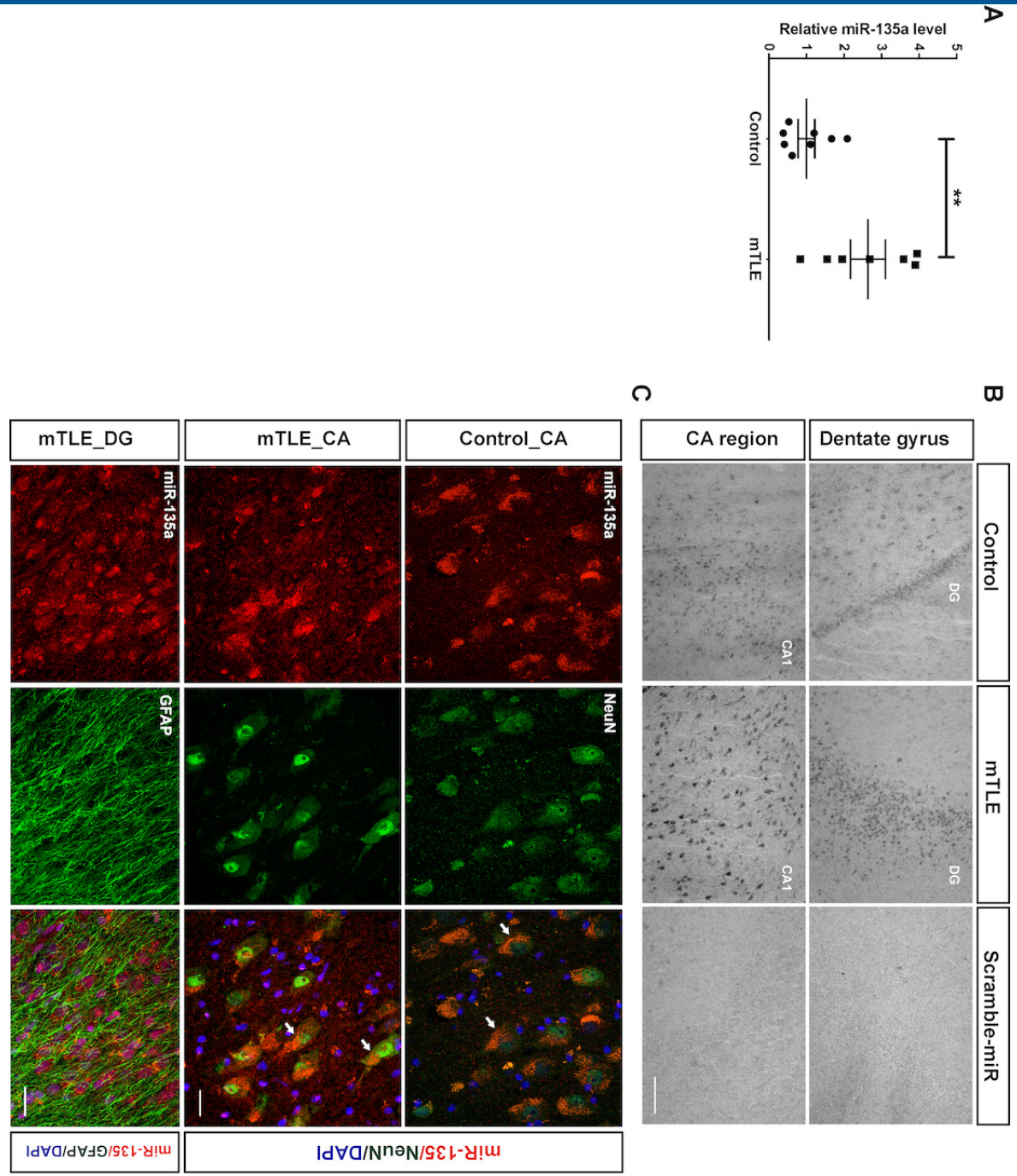
A
Relative miR-135a level
5
4
3
2
1
0
**
Control
mTLE
B
Control
mTLE
Scramble-miR
Dentate gyrus
CA region
DG
CA1
C
Control_CA
mTLE_CA
mTLE_DG
miR-135a
NeuN
GFAP
miR-135/NeuN/DAPI
miR-135/GFAP/DAPI

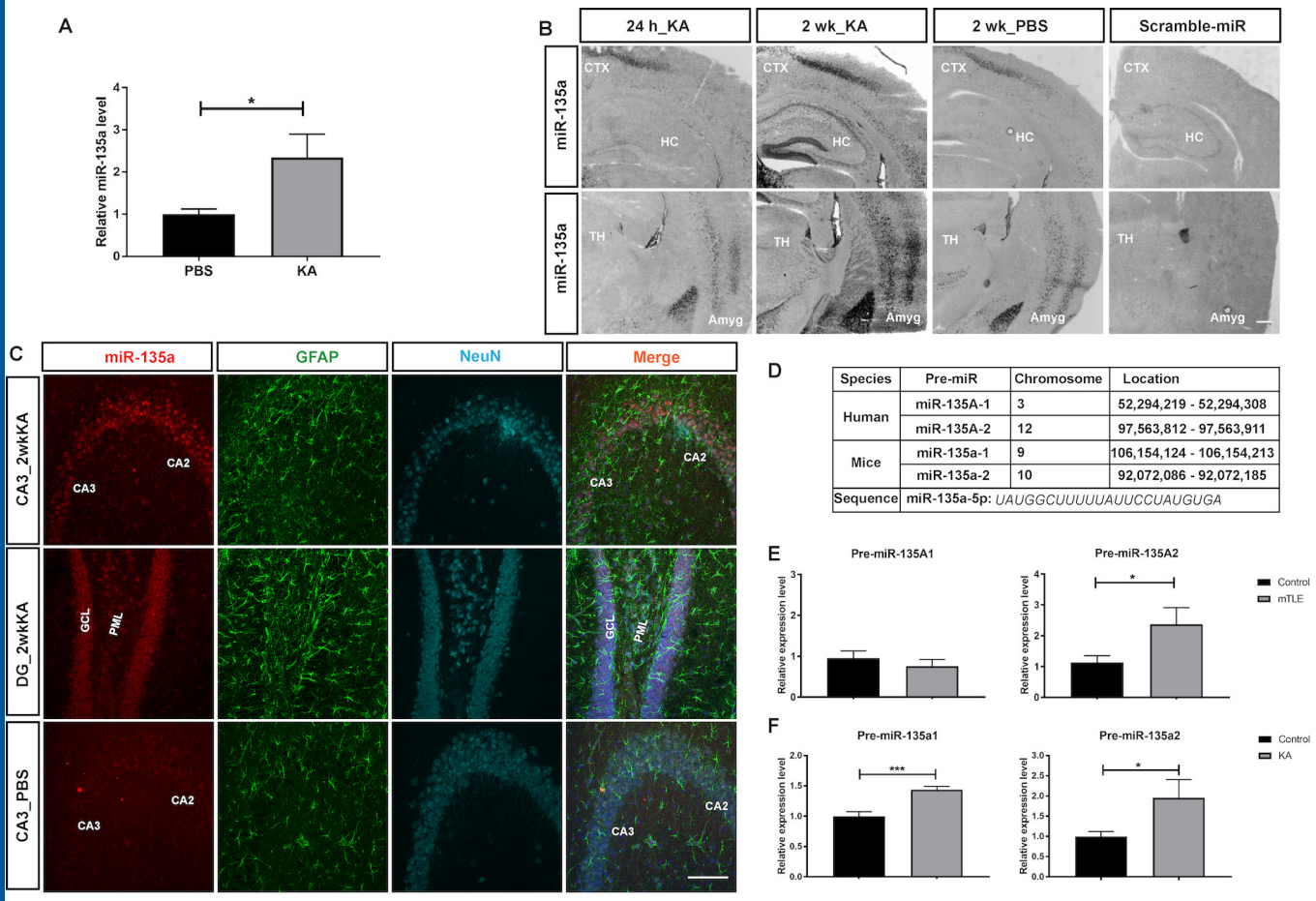


| Species | Pre-miR | Chromosome | Location |
|---|---|---|---|
| Human | miR-135A-1 | 3 | 52,294,219 - 52,294,308 |
| | miR-135A-2 | 12 | 97,563,812 - 97,563,911 |
| Mice | miR-135a-1 | 9 | 106,154,124 - 106,154,213 |
| | miR-135a-2 | 10 | 92,072,086 - 92,072,185 |
| Sequence | miR-135a-5p: *UAUGGCUUUUUAUUCCUAUGUGA* | | |

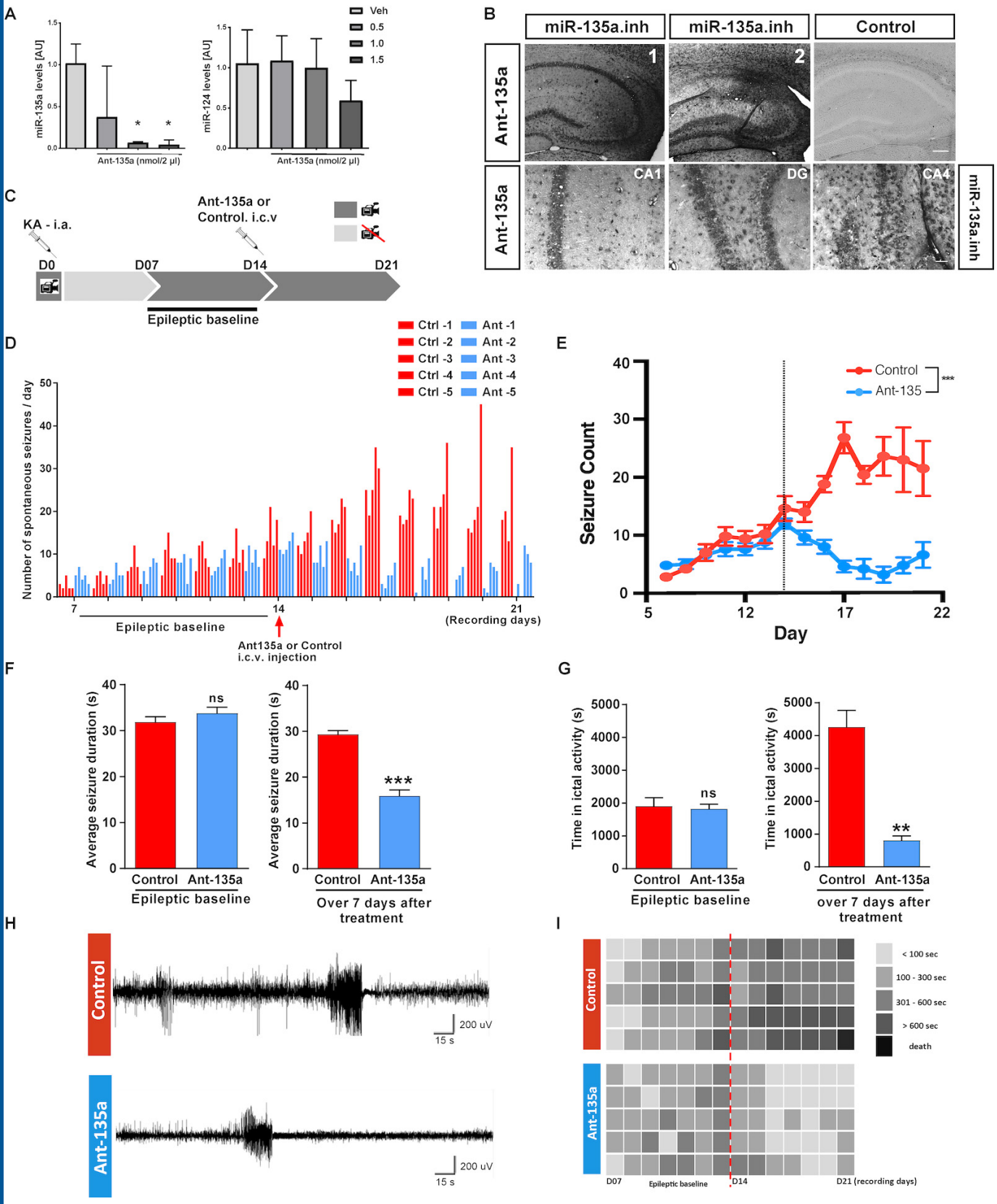

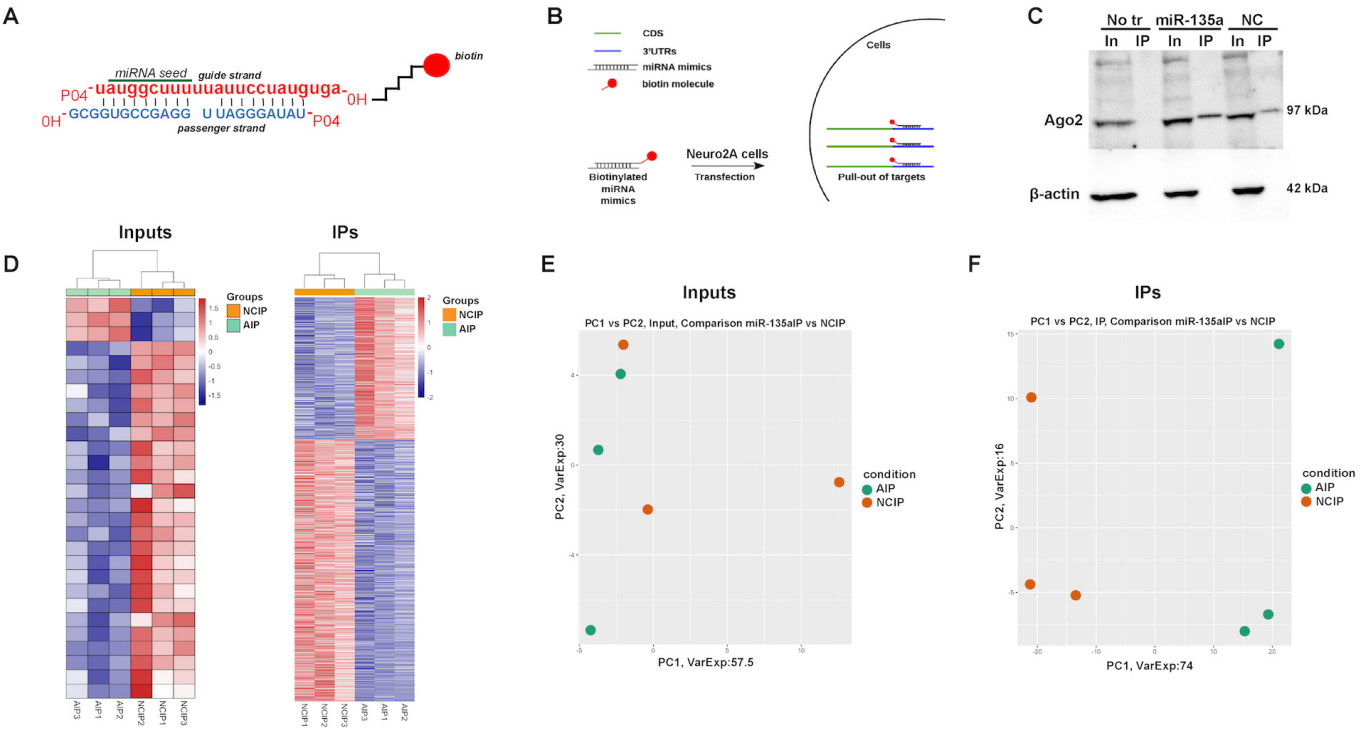

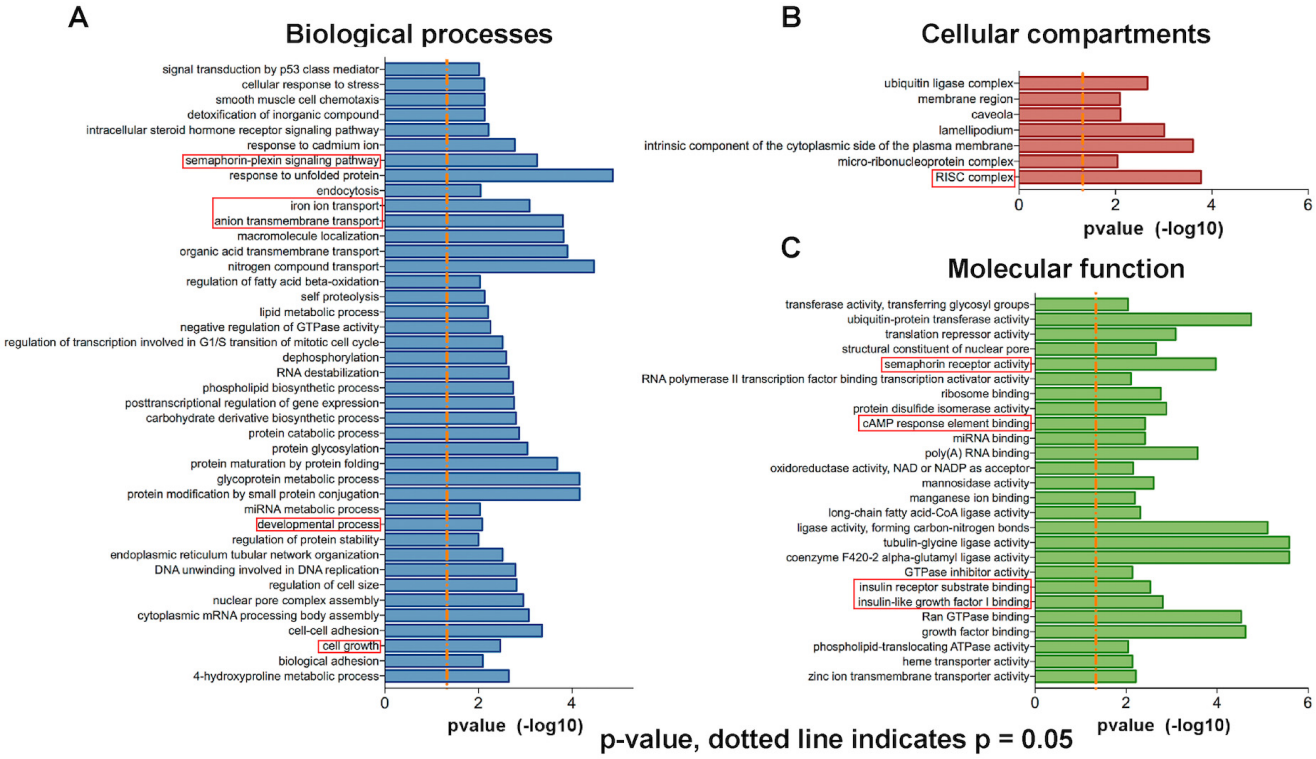


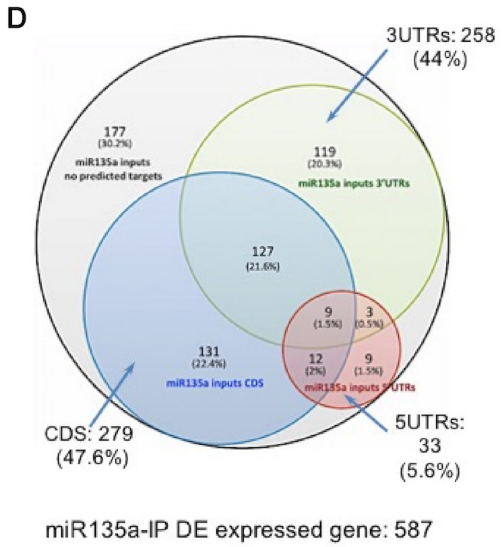


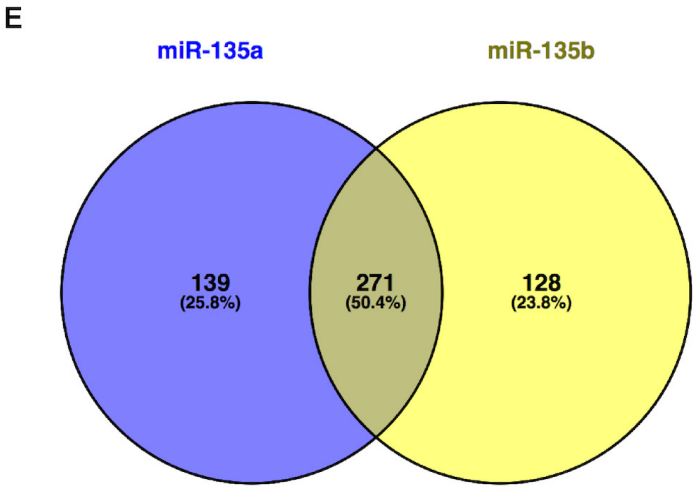

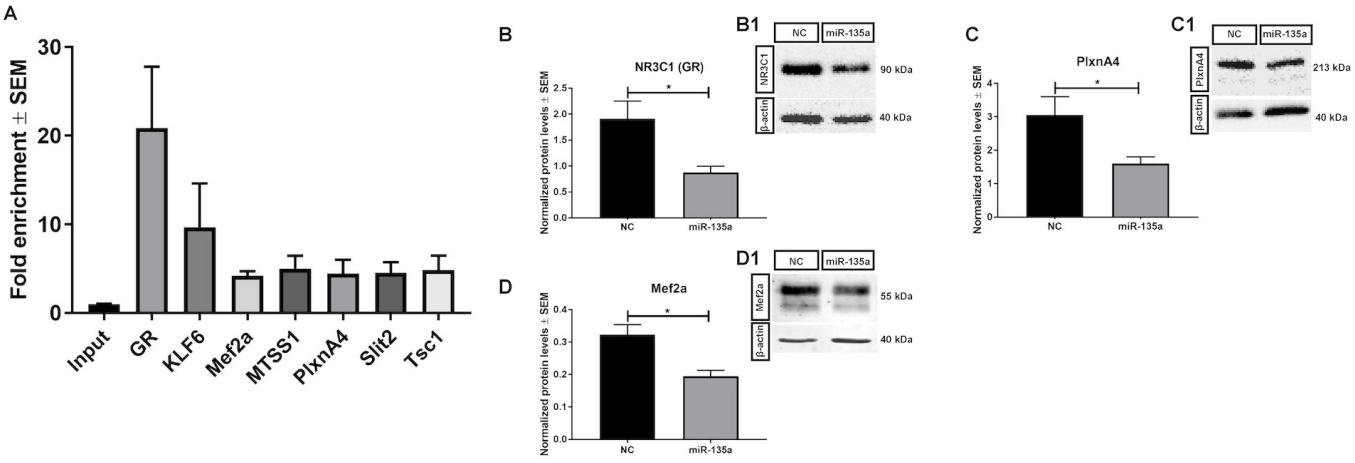

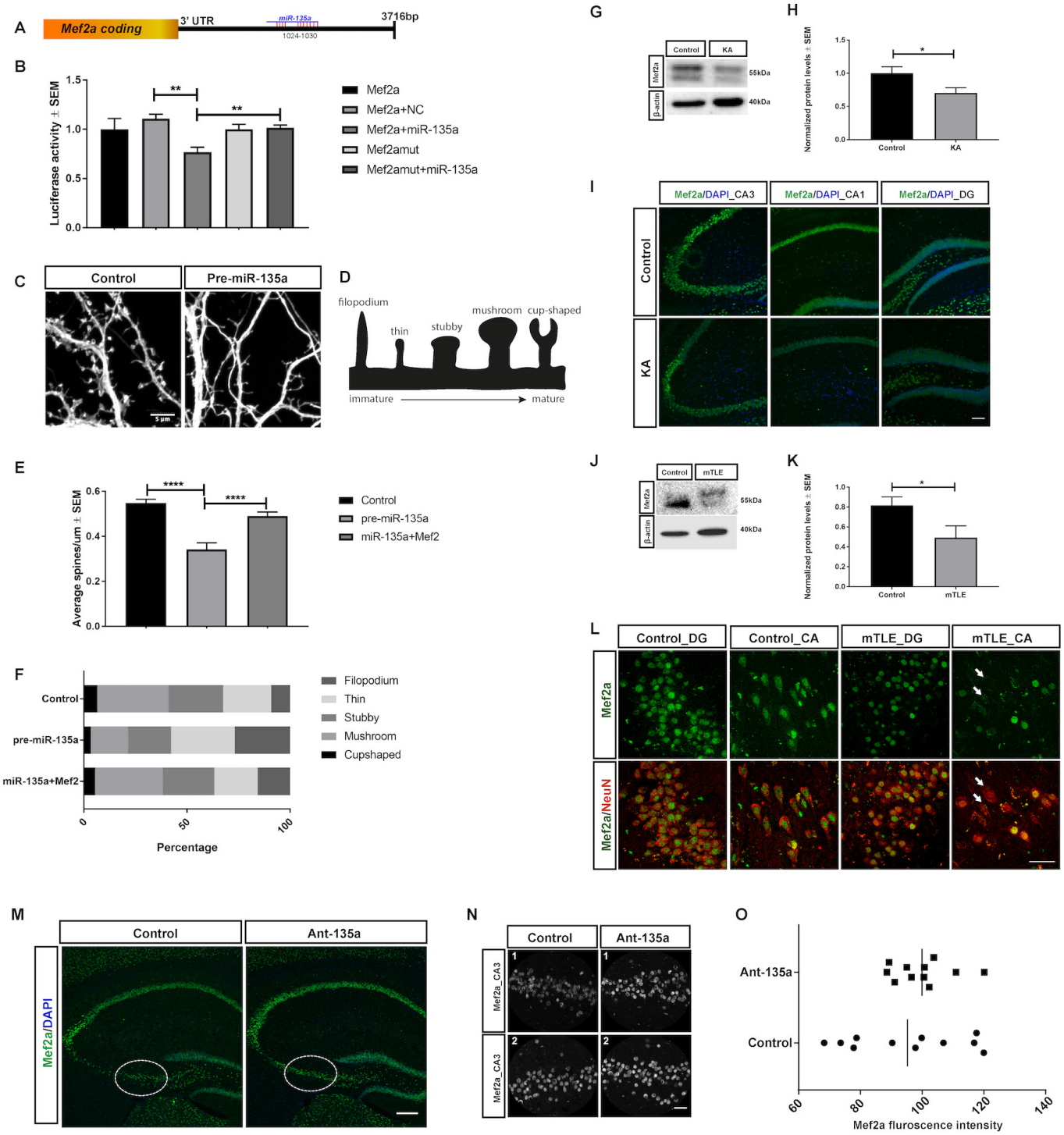

**Table 1**: **Details of control and mTLE patients used in this study**.

| Number | Sample | Age | Sex | PMD | Age of onset | Years of epilepsy | AED's |
|---|---|---|---|---|---|---|---|
| 1 | Control | 58 | M | 7 hr | NA | NA | NA |
| 2 | Control | 73 | F | 6,5 hr | NA | NA | NA |
| 3 | Control | 71 | M | 9 hr | NA | NA | NA |
| 4 | Control | 62 | M | 7 hr | NA | NA | NA |
| 5 | Control | 64 | F | 4,5 hr | NA | NA | NA |
| 6 | Control | 74 | M | 8 hr | NA | NA | NA |
| 7 | Control | 94 | F | 4 hr | NA | NA | NA |
| 8 | Control | 70 | M | 20,5 hr | NA | NA | NA |
| 9 | Control | 82 | M | 4 hr | NA | NA | NA |
| 10 | Control | 94 | M | 5 hr | NA | NA | NA |
| 11 | Control | 78 | F | 7 hr | NA | NA | NA |
| 12 | Control | 93 | M | 7,5 hr | NA | NA | NA |
| 13 | Control | 72 | F | 7 hr | NA | NA | NA |
| 14 | Control | 75 | F | 9 hr | NA | NA | NA |
| 1 | TLE-HS | 41 | M | NA | 1 | 40 | CBZ |
| 2 | TLE-HS | 36 | F | NA | 14 | 22 | OXC, LZP |
| 3 | TLE-HS | 42 | M | NA | 0,45 | 41 | LEV, LTG |
| 4 | TLE-HS | 52 | F | NA | 20 | 32 | CBZ, CLO, DZP |
| 5 | TLE-HS | 50 | M | NA | 2,5 | 47 | LTG, CBZ, CLO |
| 6 | TLE-HS | 41 | M | NA | 10 | 31 | PHT, CLO, CBZ, LTG |
| 7 | TLE-HS | 49 | F | NA | 12 | 37 | OXC, CLO, SER |
| 8 | TLE-HS | 58 | F | NA | 36 | 22 | LEV, LTG |
| 9 | TLE-HS | 23 | F | NA | 14 | 9 | LTG |
| 10 | TLE-HS | 60 | F | NA | 15 | 45 | LTG, CBZ, LEV |
| 11 | TLE-HS | 41 | M | NA | 16 | 25 | PGB, RES, CBZ |

Abbreviations: F, female; hr, hour; M, male; NA, not applicable. Details of medication: LTG, lamotrigine; PHT, phenytoin; CBZ, carbamazepine; LEV, levetiracetam; OXC, oxcarbazepine; CLO, clobazam; DZP, diazepam; LZP, lorazepam; SER, Seroquel; PGB, pregabaline; RES, restoril.

**Table 2: List of primers and their sequences used in the study.**

| | | Primer sequence | |
|---|---|---|---|
| Species | Target | forward | reverse |
| Mouse | Nr3c1 (GR) | GGGGAAGCGTGATGGACTTG | CAGCAGCCACTGAGGGTGAA |
| Mouse | Klf6 | GAGTTCCTCCGTCATTTCCA | GTCGCCATTACCCTTGTCAC |
| Mouse | Mef2a | AGCAGCACCATCTAGGACAA | CTGCTGTTGGAAGCCTGATG |
| Mouse | Mtss1 | ACAGCACCCAGACCACCACC | TGCCTCCTGGTCGCCACTTA |
| Mouse | PlxnA4 | TCTCAGTACAACGTGCTG | TAGCACTGGATCTGATTGC |
| Mouse | Slit2 | CAGTCATTCATGGCTCCCTC | TTCCCTCGGCAGTCTACAAT |
| Mouse | Tsc1 | CAGGAGTTACAGACAAAGCTG G | AGCTTCTGAGAGACCTGGCT |
| Mouse | Gapdh | CCCCAATGTGTCCGTCGTG | GCCTGCTTCACCACCTTCT |
| Human | Pre-miR-135a1 | TCGCTGTTCTCTATGGCTTTT | CGGCTCCAATCCCTATATGA |
| Human | Pre-miR-135a2 | TGCTTTATGGCTTTTTATTCCT | TGGCTTCCATCCCTACATGA |
| Human | GAPDH | TGGAAGGACTCATGACCACA | GGGATGATGTTCTGGAGAGC |
| Mouse | Pre-miR-135a1 | GCCTCACTGTTCTCTATGGCTT T | CCACGGCTCCAATCCCTATATG A |
| Mouse | Pre-miR-135a2 | TGCTTTATGGCTTTTTATTC | CATCCCTACATGAGACTTTATT |
| Mouse | β-actin | AGCCATGTACGTAGCCATCC | CTCTCAGCTGTGGTGGTGAA |

**Table 3: List of several experimentally validated targets of miR-135a that were enriched in the bio-IP samples.**

| Target | Name | Reference |
|---|---|---|
| Mtss1 | Metastasis suppressor protein 1 | (Zhou et al., 2012) |
| Cdk4 | Cyclin-dependent kinase 4 | (Dang et al., 2014) |
| Vcan | Proteoglycan Versican | (Zhao et al., 2017) |
| Zfp217 | Zinc finger protein 217 | (Xiang et al., 2017) |

**Table 4: Selection of targets identified by bio-IP with important roles in the regulation of epilepsy-relevant processes and pathways**.

| Gene | Function | Log FC | P-value | FDR |
|---|---|---|---|---|
| Nr3c1 (GR) | Glucocorticoid receptor | 3,37865036 | 8,86E-16 | 2,17E-13 |
| Tsc1 | Tuberous sclerosis complex | 1,37190519 | 0,00050763 | 0,00589048 |
| Nrp1 | AG, MFS | 1,3675057 | 7,45E-06 | 0,00017204 |
| Tgfbr1 | TGFbeta signalling | 1,35700473 | 1,27E-06 | 3,73E-05 |
| Mtss1 | Spine density | 1,3275843 | 0,00238517 | 0,02018217 |
| PlxnA4 | AG, MFS | 1,20703562 | 0,00012557 | 0,00190651 |
| Cacna1c | Calcium channel | 1,1901732 | 0,00076192 | 0,00819715 |
| Ncam1 | Neurite outgrowth | 1,05245567 | 5,18E-05 | 0,00092656 |
| Slit2 | AG, MFS | 1,04442804 | 0,00033258 | 0,00418342 |
| Mef2a | Spine density | 0,983455 | 0,00203267 | 0,01769962 |
| Creb1 | Transcription factor | 0,90909684 | 0,00363345 | 0,02809798 |

These targets were selected based on their function involving in key neuronal functions. AG, axon guidance; MFS, mossy fiber sprouting.